ISSN: 3069-3209
Research Article
Current Research in Civil and Mechanical Engineering

A Research Road Map Approaching Thin Films of Semiconductors
Electropulsing Induced Phase Transformations in Alloys and Thin Films of TCO and TE Semiconductors

Yaohua Zhu

Dept. of Industrial and Systems Engineering, The Hong Kong Polytechnic University, China

*Corresponding author: Yaohua Zhu, Dept. of Industrial and Systems Engineering, The Hong Kong Polytechnic University, China.

Submitted: 12 March 2025 **Accepted:** 22 March 2025 **Published:** 28 March 2025

https://doi.org/10.63620/MKCRCME.2025.1002

Citation: *Zhu, Y. (2025). A Research Road Map Approaching Thin Films of Semiconductors Electropulsing Induced Phase Transformations in Alloys and Thin Films of TCO and TE Semiconductors. Curre Res in Civil & Mech Eng, 1(1), 01-23.*

Abstract

Based on systematic studies of equilibrium and non-equilibrium transformations and the stress induced transformations, studies of electropulsing induced phase transformations of alloys and thin films of semiconductors, such as transparent conductive oxides (TCO) and thermoelectric (TE) materials: Bi-Te, AZO-2 and AZO-5 have been carried out. As an advanced process, electropulsing increases plastic elongation of alloys about 437%. Under adequate electropulsing, phase transformations and microstructural changes were tremendously accelerated by factors of at least 6000 times, compared to conventional aging processes in alloys. The electropulsing induced circular phase transformations (quenching – up quenching, up quenching – quenching, ... quenching – up quenching – quenching – up quenching etc.) and preferred crystal orientation changes are quantitatively detected to complete several seconds, in the alloys and the thin films of the AZO and Bi-Te semiconductors. Adequate electro pulsing increases electric conductivity of the thin-films of the semiconductors for 44.6% and 28.5%, respectively. The quantitative detection of multi-circulation of both phase transformations and preferred crystal orientation changes makes it possible to monitor microstructural changes and to enhance physical and optical properties and upgrade the currently applied thin films, microchips and strips etc. to a new level in the large market of the semiconductors.

Introduction

Most materials are subjected to one or more thermal or thermo-mechanical processes in their manufacturing or in subsequent service. The microstructure changes and phase transformations which occur during thermal and thermo-mechanical processes can vary greatly, depending on the materials involved and the particular conditions to which they are subjected. Properties and therefore applications, are closely linked to those phase transformations which cause the development of useful microstructures, therefore properties may depend in a sensitive way on manufacturing processes and the conditions of service.

Practical research in physical metallurgy is largely an examination of the phase relationships which occur in different materials, and their effects on the microstructure of alloys during thermal or thermo-mechanical processing.

Results and Discussion

Systematic researches started with establishing the equilibrium phase diagrams for binary Zn-Al, ternary Zn-Al-Si and Zn-Al-Cu, and quaternary Zn-Al-Cu-Si alloy systems, (Fig.1) [1]. This was followed by studied of the phase transformations which occurred in solution-treated alloys of different compositions, i.e. Al-rich, monotectoid and eutectoid alloys, (Fig.2). Intrinsic relationships between equilibrium and non-equilibrium phase transformations were determined, which led to the development of a General Rule for Phase Transformation in Zn-Al Based Alloys [2].

Further studies extended the work to cover various complex non-equilibrium practical processes, such as casting, rapid-solidification, furnace cooling, continuously casting, welding, al-

loying and the use of rare-earths alloying [3].

This was followed by the results of extensive investigations which were carried out on stress-induced phase transformations and their effects on microstructure. Various thermo- mechanical processes, such as extrusion, tensile, creep, fatigue, impact, damping, milling, rolling, cold-drawing and ultra-precision machining etc., were involved in the investigation, Fig.3-5.

Mechanical and physical behaviors, such as plastic deformation, super plasticity, fracture mechanisms, mechanical properties, dimensional stability and wear resistance etc., were discussed from point of view of phase transformation and microstructural change, (Fig.3-5).

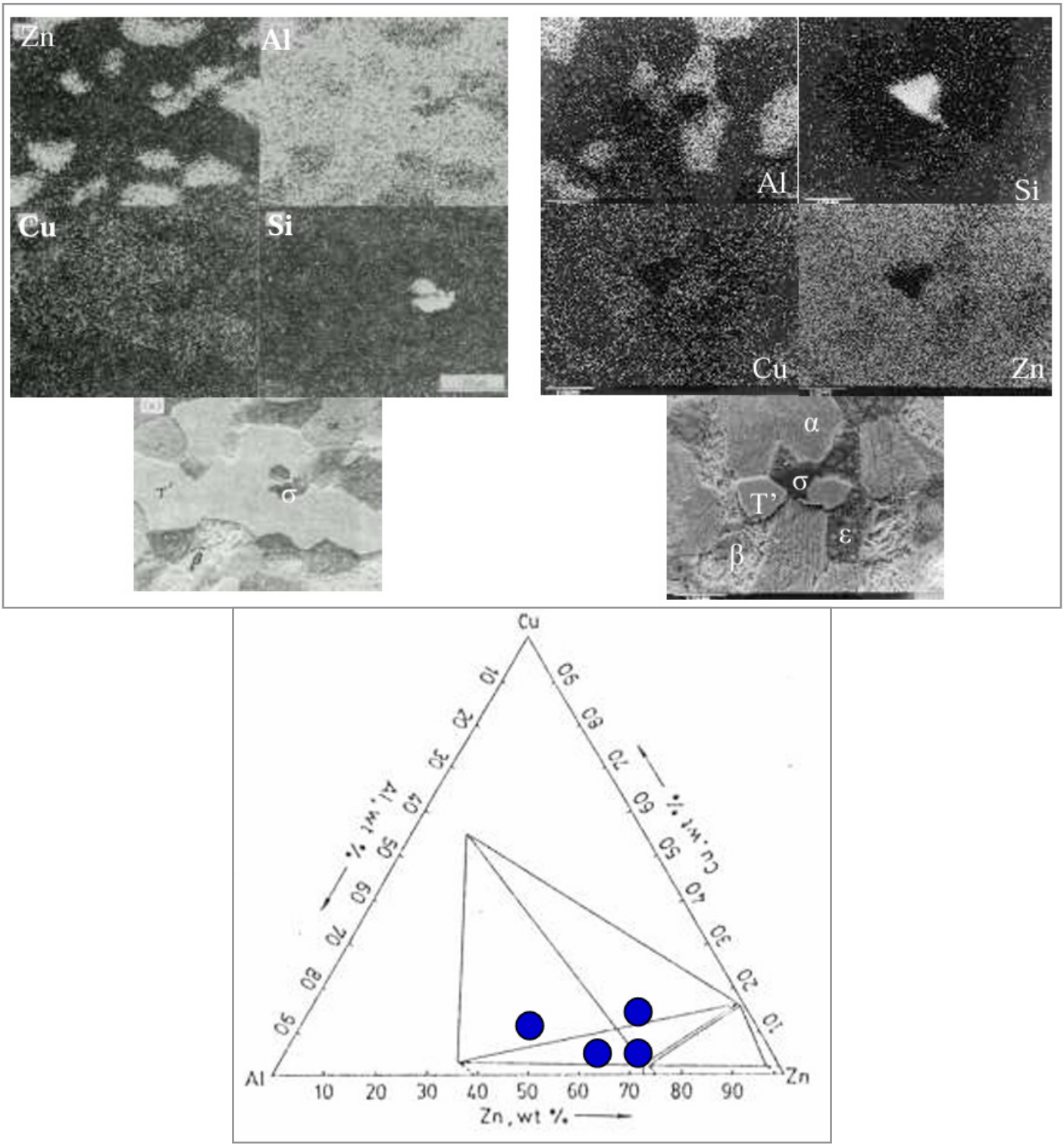

Figure 1: BSEM image and mappings of Zn, Al, Cu and Si of the specimens 3 and 4, showing β + T' == α + ε at 285°C Equilibrium, according to the Phase Rule: 3 components 4 phases co-existence Freedom = 0 with Si stable phase.

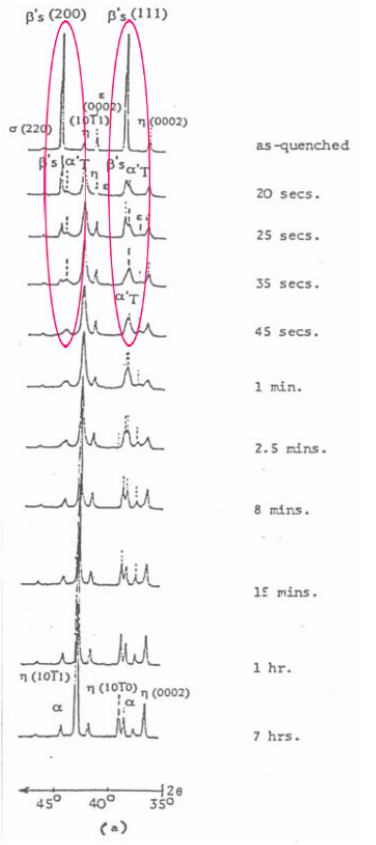

X-ray diffractograms of alloyAlZn75Cu3Si2ageing at 100^{O}C, Showing a cellular reaction at the early stage of ageing.

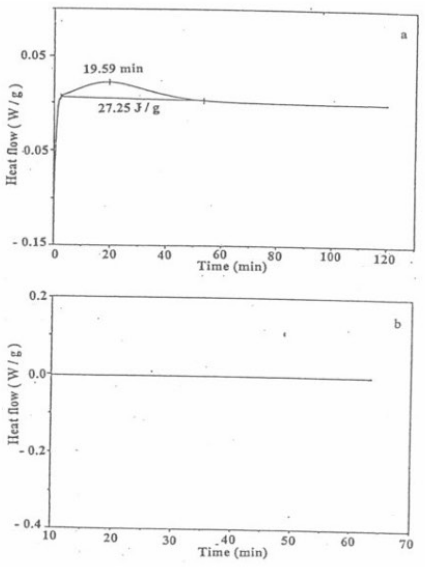

Exothermal heat flow of alloy ZnAl22Cu2 during quench-ageing at 50^{O}C (a) and 200 ^{O}C (b).

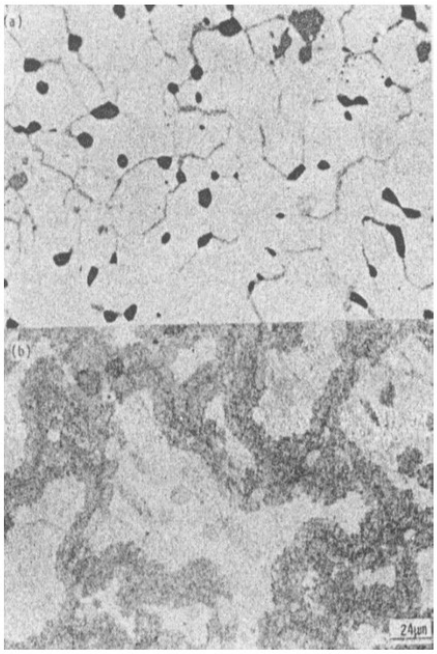

Optical micrographs of alloyAlZn75Cu3Si2 after ageing at 100^{O}C for 0.5 min., showing the development of discontinuous precipitation at grain boundries.

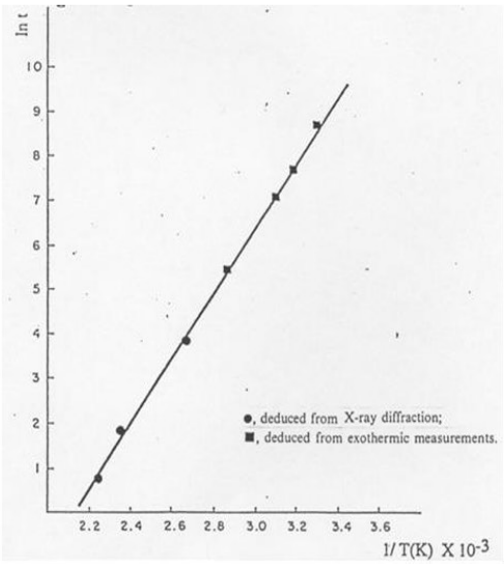

Arrhenius plot for determination of activation energy of determination of β'$_s$-phase in alloy ZnAl22Cu2 deduced from X-ray diffraction and from exothermal measurement (DSC)..

Figure 2: β's → α'T + ε + η detected by XRD and DSC

The two kinds of phase transformation were observed in various external stresses (such as tensile, creep, fatigue, milling, ultra-precision machining, and mechanical alloying etc.) deformed Zn-Al based alloy specimens. The decomposition of the η'T

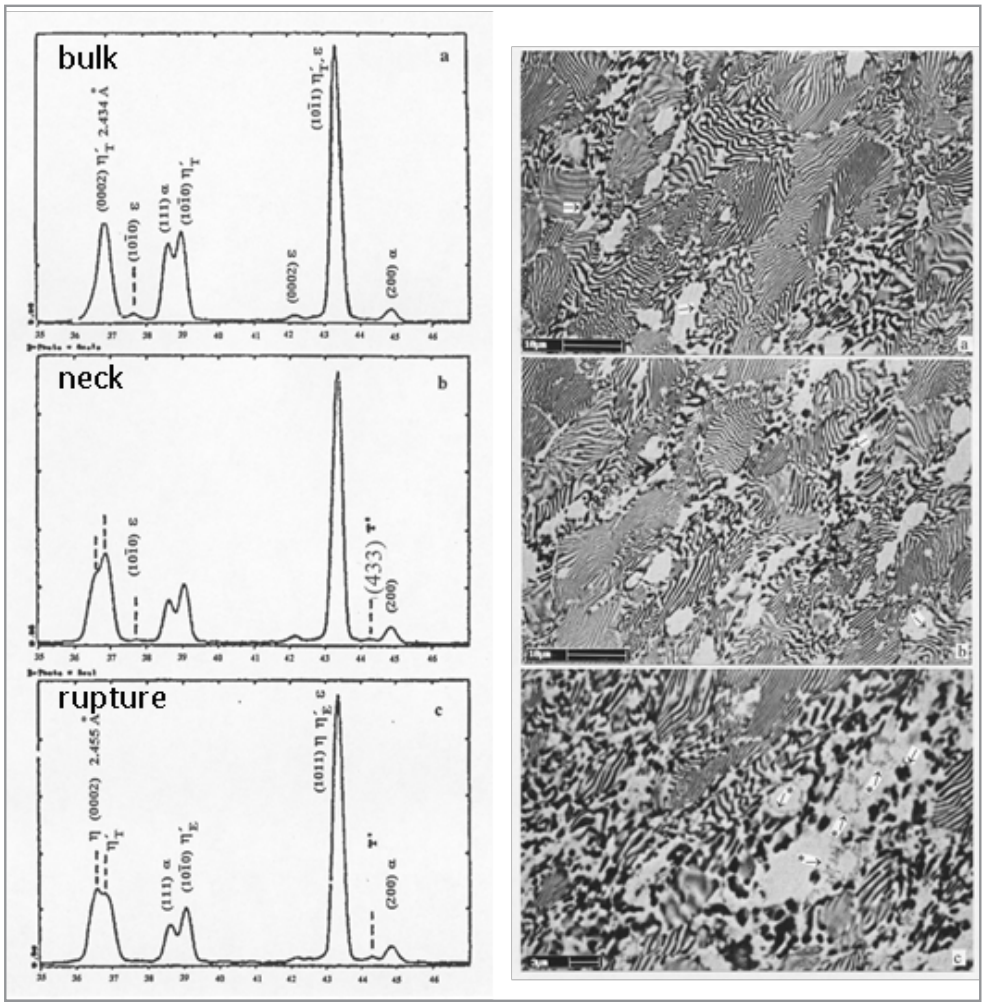

Figure 3: XRD and BSEM images of extruded ZA alloy specimens after tensile deformation.

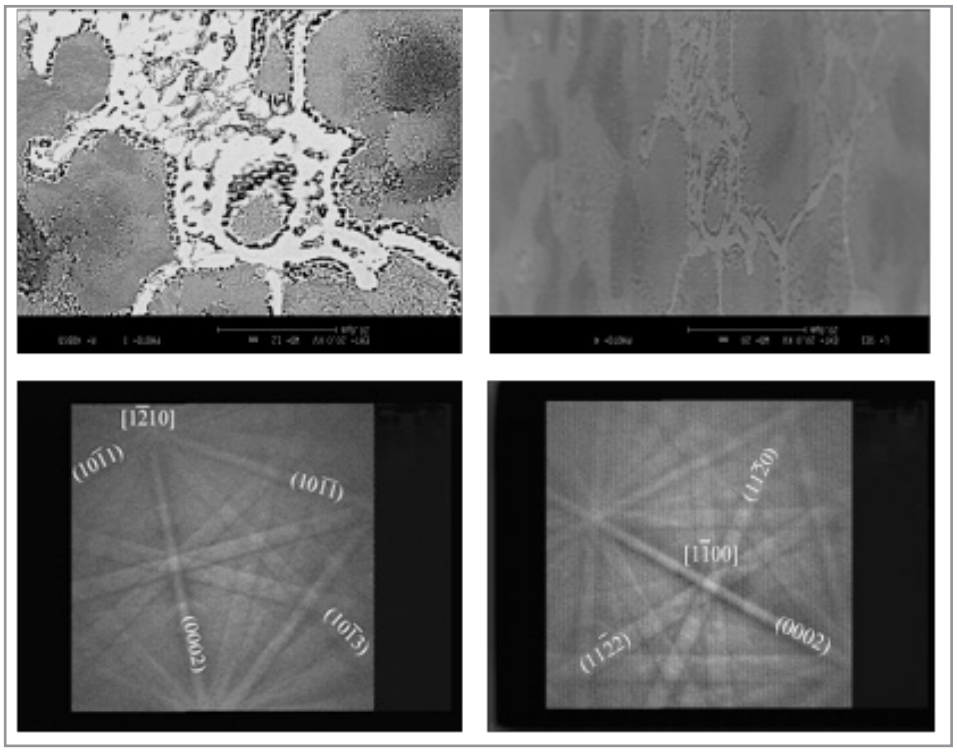

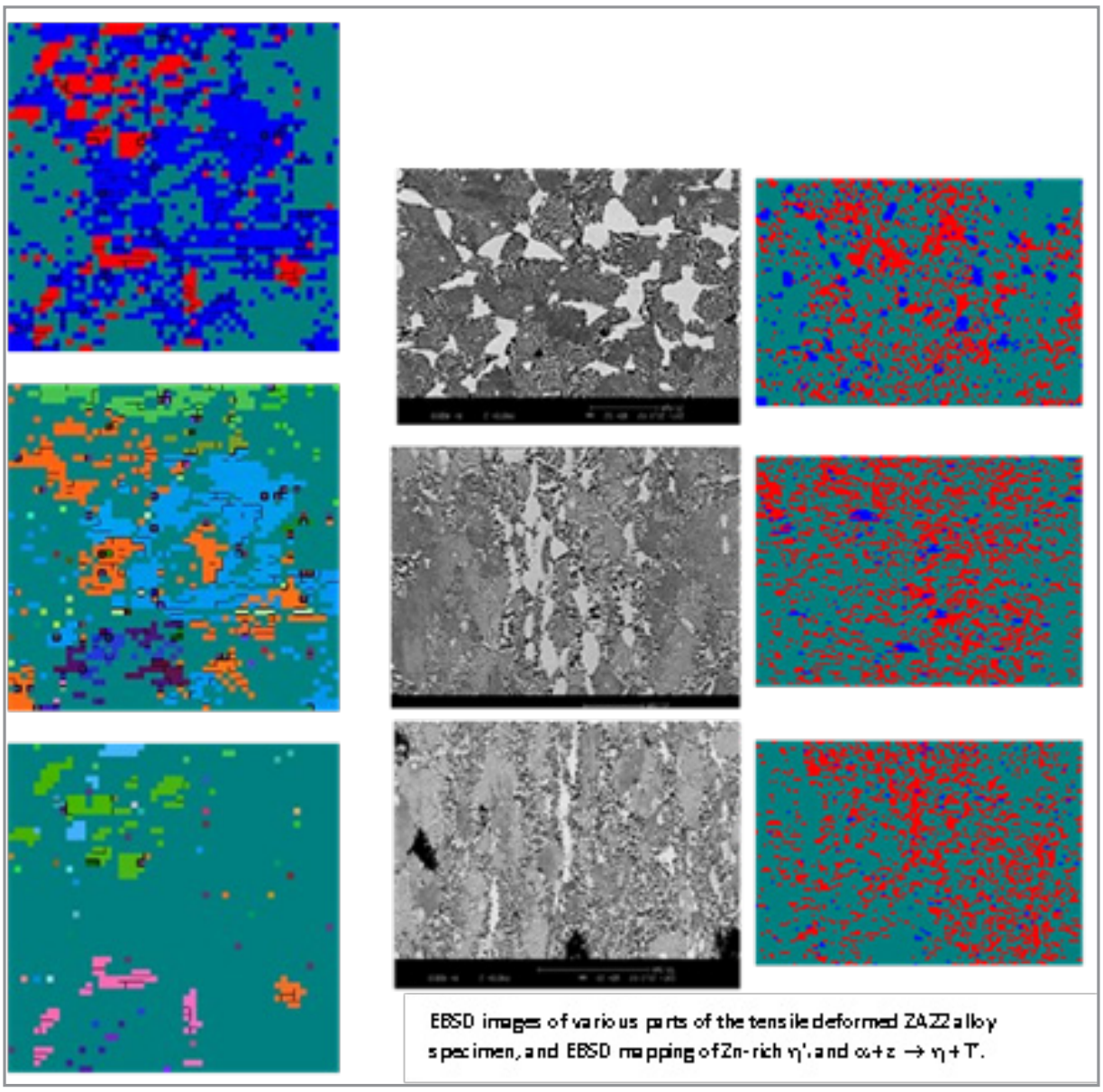

Figure 4: External stress induced phase transformation (BSEM and EBSD) in furnace cooled extruded ZA alloy specimens after tensile deformation.

phase occurred in the bulk part of the specimen, while the four-phase transformation was observed in the neck zone, and well developed in the strain concentrated rupture part of the specimen. As shown in Fig.3, the two kinds of precipitates are indicated by arrows → and *→, respectively

As a consequence, it was reasonable to elucidate that there was an intrinsic co-relationship of phase transformations in the aged and the external stress deformed alloy specimens, i.e. the second General Rule of Phase Transformation in Zn-Al based alloys (II) – On external stress-induced phase transformation was summarized as follows,

" The phase transformation occurred in the less external strain part of the specimen was related with the early stage of phase transformation during aging (processes without external stress), while the phase transformation occurred during the prolonged aging corresponded to that observed in the external strain concentrated parts of the specimen, such as the neck zone and the rupture part of the specimen ", schematically shown in Fig.5.

Solid lines _ present the correlation between the equilibria and the phase transformations in the isothermal processes, the _ • _ lines present the correlation between the phase transformations in the isothermal processes and the external stress induced phase transformations, and the dashed lines imply the correlation between the equilibria and the external stress induced phase transformations [5].

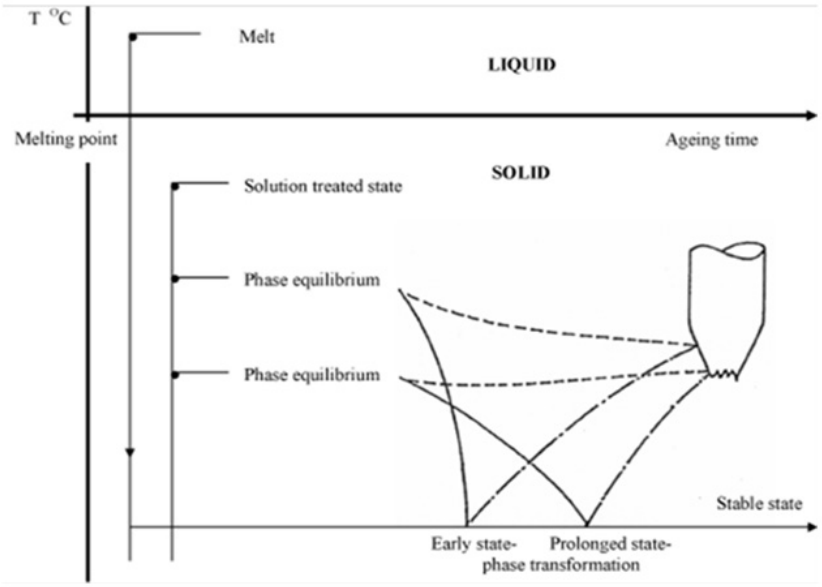

Figure 5: Co-relationships between the phase equilibriums and both of the phase decompositions, which occurred in the thermal and thermos-mechanical processes:
__ __ the correlations between the equilibrium and the phase transformations in the isothermal processes
__•__ the correlation between the phase transformations under external stress and without external stresses
------- the correlation between the equilibriums and phase transformations with external stresses

The studies on ultra-precision machining (UPM) induced phase transformation and plastic deformation, which appeared critical for the surface properties of the alloy specimens, as shown in Fig.6, is of important significance in practical applications. The schematic geometry of UPM is shown in Fig.6 [6].

UPRM (ultra-precision raster milling) asserts an external stress onto the surface of the alloy, which results in phase transformations and in changes of crystal orientation [7, 8]. A layer of plastic deformation of about 250 nm was detected at the surface of the UPRM Zn-Al based alloy (ZA22). Within the surface layer of 250 nm, the plastic deformation was enhanced with increasing feeding rate up to 60 mm/min under S4000 rpm and depth of cut (DoC) of 30 μm. Accordingly the decomposition of the η'FC with an activation energy of 71.5 kJ mol-1 was accelerated. Upon the feeding rate increased to 100 mm/min, shear deformation occurred. Meanwhile the plastic deformation disappeared at the surface of the UPRM alloy specimens.

Within the surface layer of about 250 nm thickness, the plastic deformation was reduced with increase in the distance from the UPM surface. Accordingly, the elastic modulus increased. When the distance from the surface was higher than 250 nm, the elastic dramatically reduced.

UPM might result in plastic deformation and hardening at the surface of the FC Zn-Al based alloy.

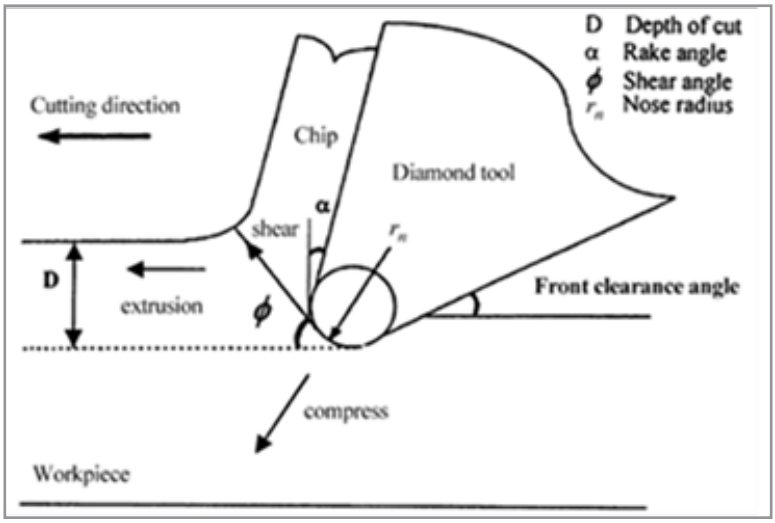

Figure 6: The schematic geometry of UPM

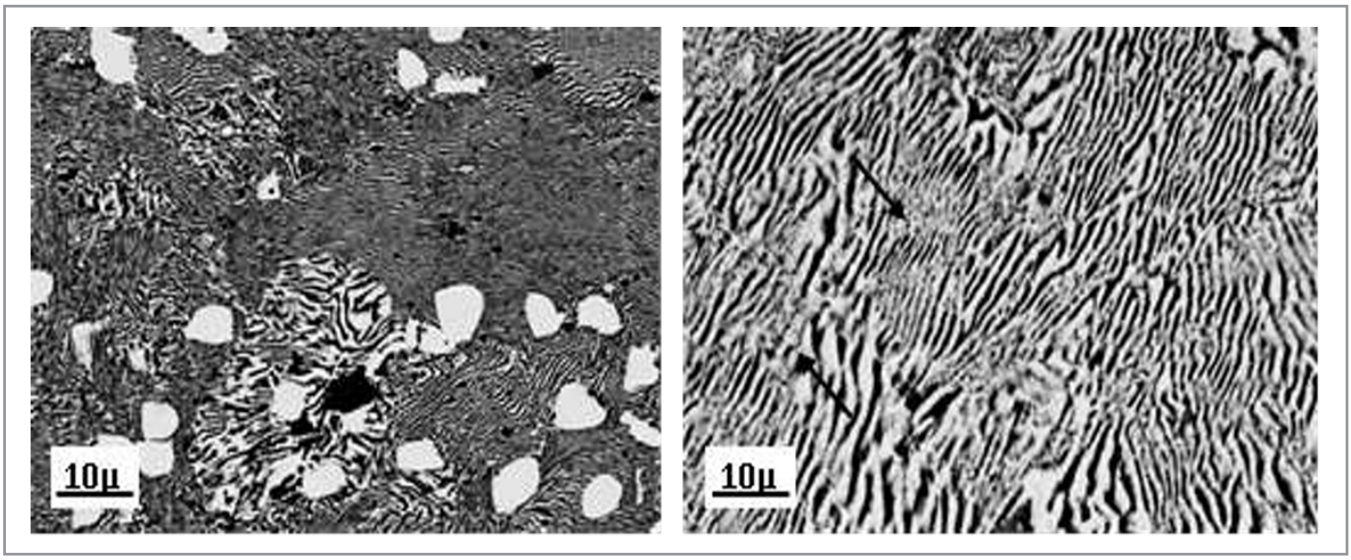

Figure 7: BSEM images of the FC ZA22 alloy specimen after ultra-precision machine at a spindle speed of 3000 rpm, a feed rate of 10 mm/min, and at various depth of cut (a) 10 µm, and (b) 20 µm.

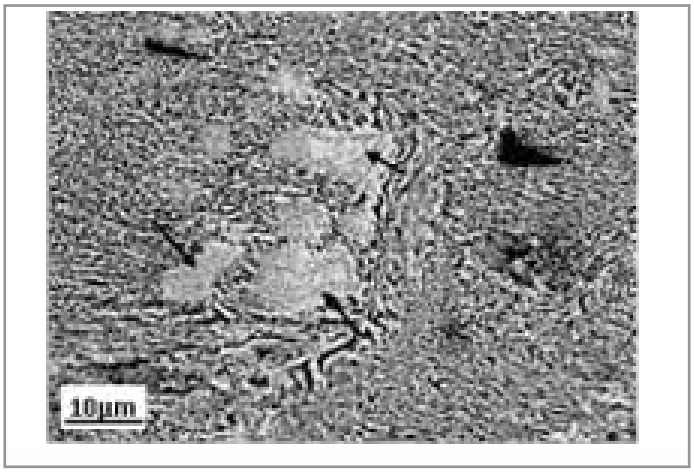

Figure 8: UPM surface of the FC ZA22 at depth of cut of 10 mm/min and a spindle speed of 3000 rpm, the grey precipitates of T' phase are indicated by arrows

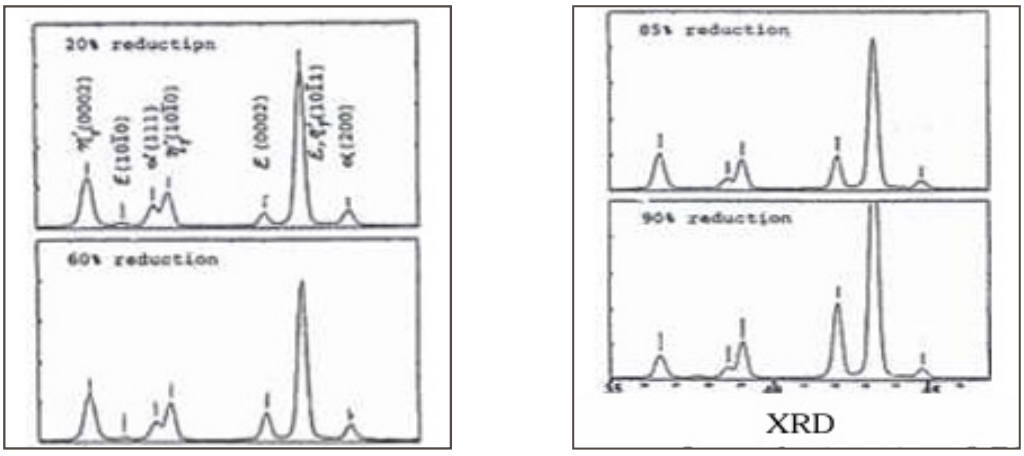

Figure 9: UPM induced changes of crystal orientation of FC ZA22 alloy specimens

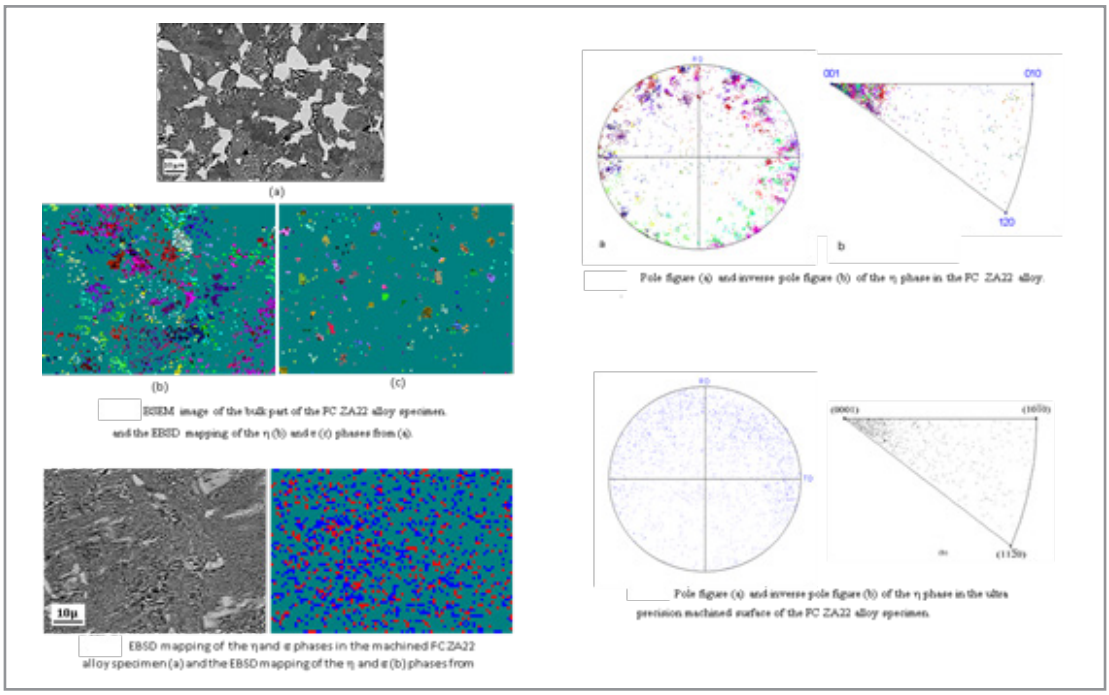

Figure 10: XRD, BSEM and EBSD mapping of FC ZA 22 alloy specimen, showing UPM induced phase transformations.

Based on systematic studies of equilibrium (Fig.1) and non-equilibrium transformations (Fig.2) and the stress induced transformations (Figs.3---10), studies of electro pulsing induced phase transformations of alloys (Figs.11-22) and thin films of semiconductors, such as transparent conductive oxides (TCO) and thermoelectric (TE) materials, such as Bi-Te, AZO-2 and AZO-5 etc. (Figs.23-30) have been conducted [9-23].

Various previously furnace cooled (FC), tempered and as mechanically deformed (AD) alloys, such as ZA22, ZA27, Mg-Al alloys (AZ91, ZA61 and AZ31) and Fe-Si steel etc., and thin films of ZA7, ZA22, ZA27, AZO, and TE were examined separately after static and dynamic electro pulsing, as shown in Table 1[17-23].

As an advanced process, electropulsing increases plastic elongation of alloy by about 437% (Fig.11), and induces circulation of plasticity changes (Fig.12). electro pulsing might tremendously enhance plastic behavior, depending on dislocation dynamics, such as accumulation and annihilation of dislocations, and phase decomposition that resulted in dislocation pinning by phase precipitates. electro pulsing accelerates dislocation movement and an adequate electro pulsing improved identity of the dislocation density, much enhanced the plasticity of the alloys [24-33]. While dislocation pinning by precipitates and transitional phases might favor both identities of microstructure (including the second phase precipitation and the residual stress etc.) and dislocation density, as a result, plastic behavior enhanced whilst the stress remained relatively high [34-38].

Table 1: Initial States of Alloys Being for Electropulsing

Initial states	Static EPT	Dynamic EPT
Furnace Cooled (FC) and tempered (with relative higher temperature) As Deformed (AD)	● ■	●
As Deformed (AD) (with relative lower temperature)	● ○ ■ ▲	● ○ ■
Magnetron sputtering coated	□ ▲ ● ○	

□ ZA7 / ● ZA22 alloy / ○ ZA27 alloy / ■ Mg alloys (AZ91,AZ61,AZ31) /

▲ Fe-Si Steels / ▲ AZO, TE thin films

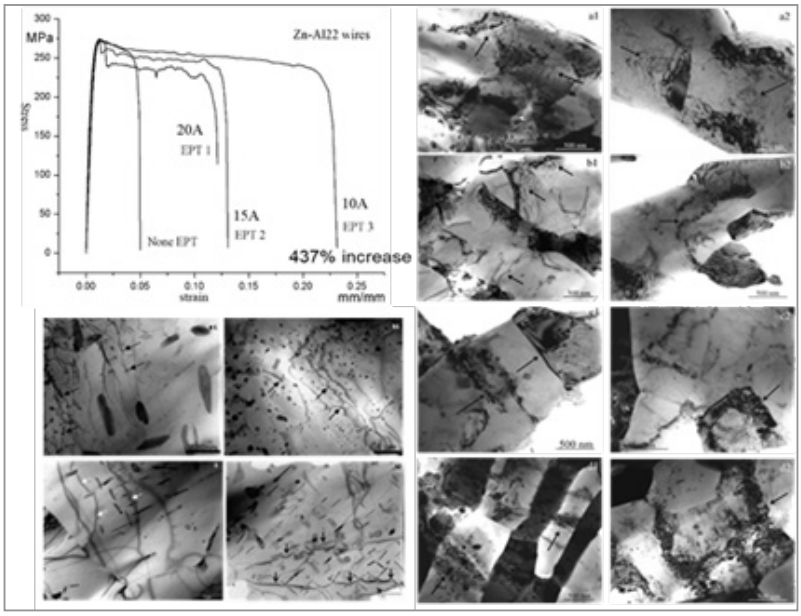

Figure 11: S-S curves of ZA22 alloy with elongation increased 437% and dislocation pinning.

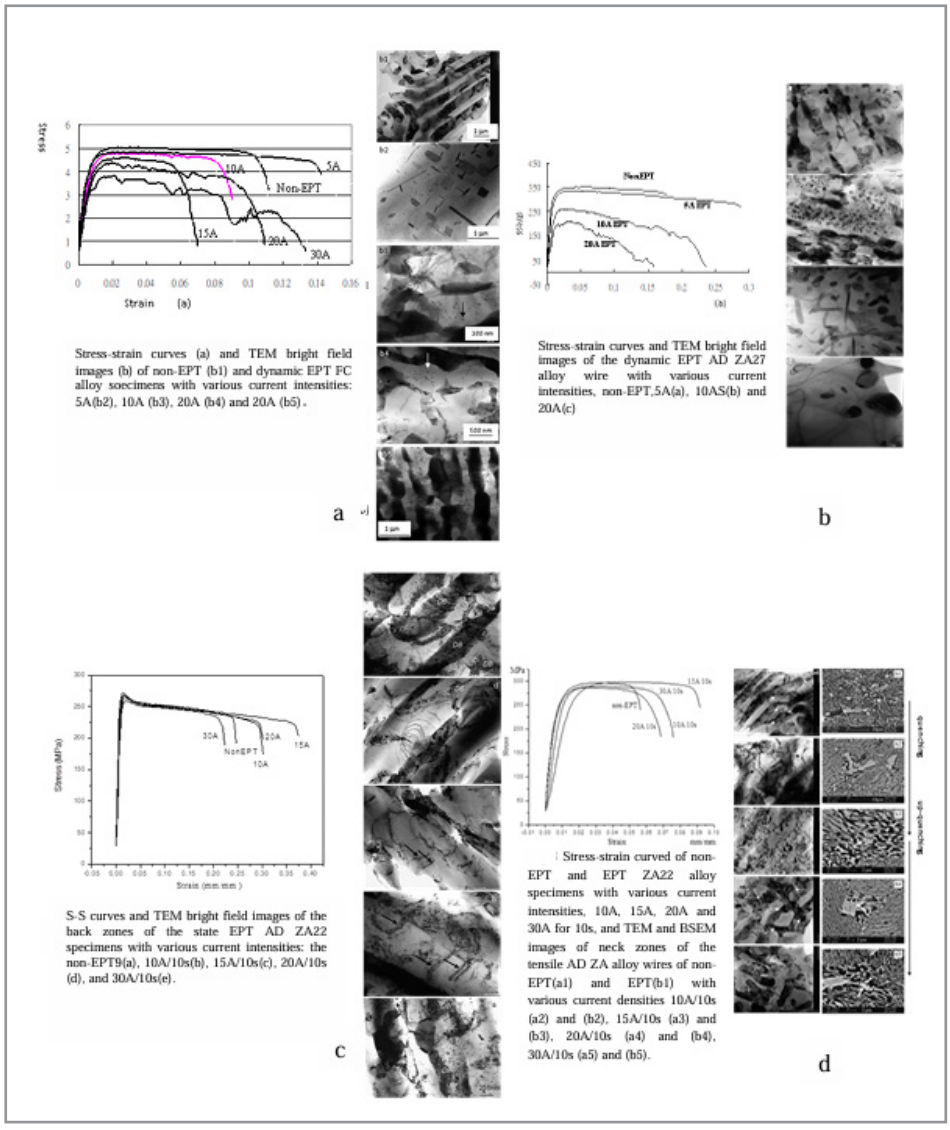

Figure 12: Electropulsing induced circulation of plasticity changes of ZA alloys, dynamic EPT FC ZA22 (a) and AD ZA27 (b), and static EPT AD ZA22 (c) and d, FC ZA22 (d).

Low temperature plastic behavior of ZA alloy under electropulsing and prompt stress responses of electropulsing are shown in Fig.13. Eletropulsing improves greatly elongation of the alloy under low temperature.

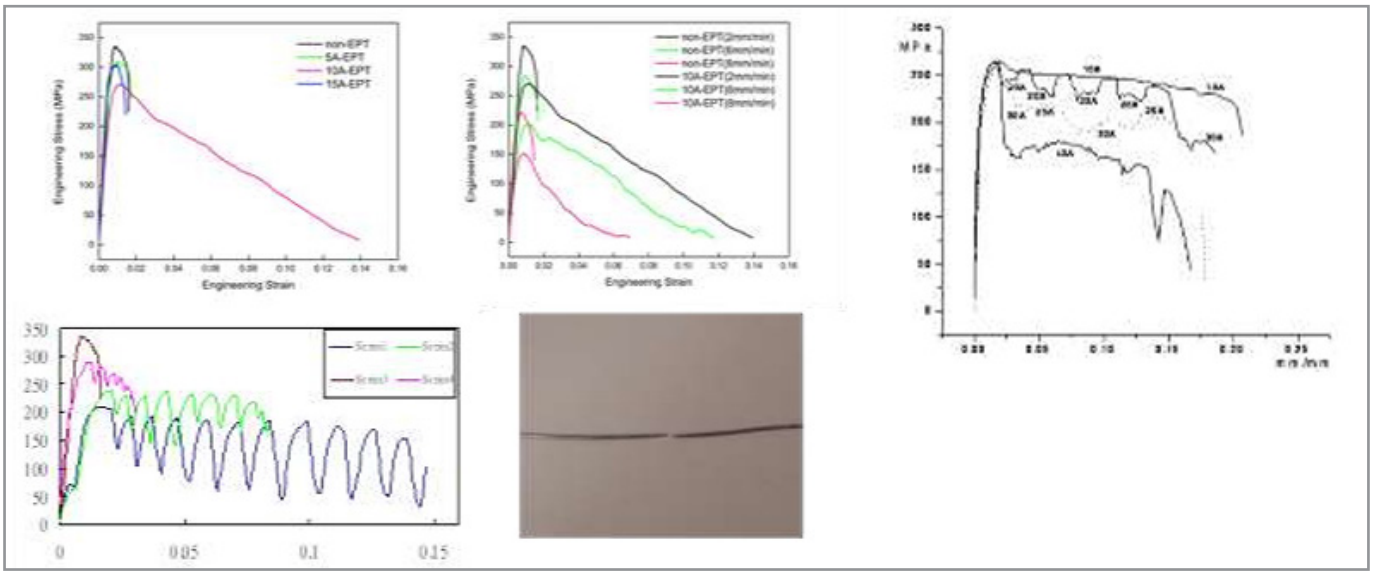

Figure 13: S-S curves of EPT ZA alloy at -60OC (a) and prompt stress responses of electropulsing (b).

Under adequate electropulsing, phase transformations and microstructural changes were tremendously accelerated by factors of at least 6000 times, compared to conventional aging processes in alloys (Fig.14).

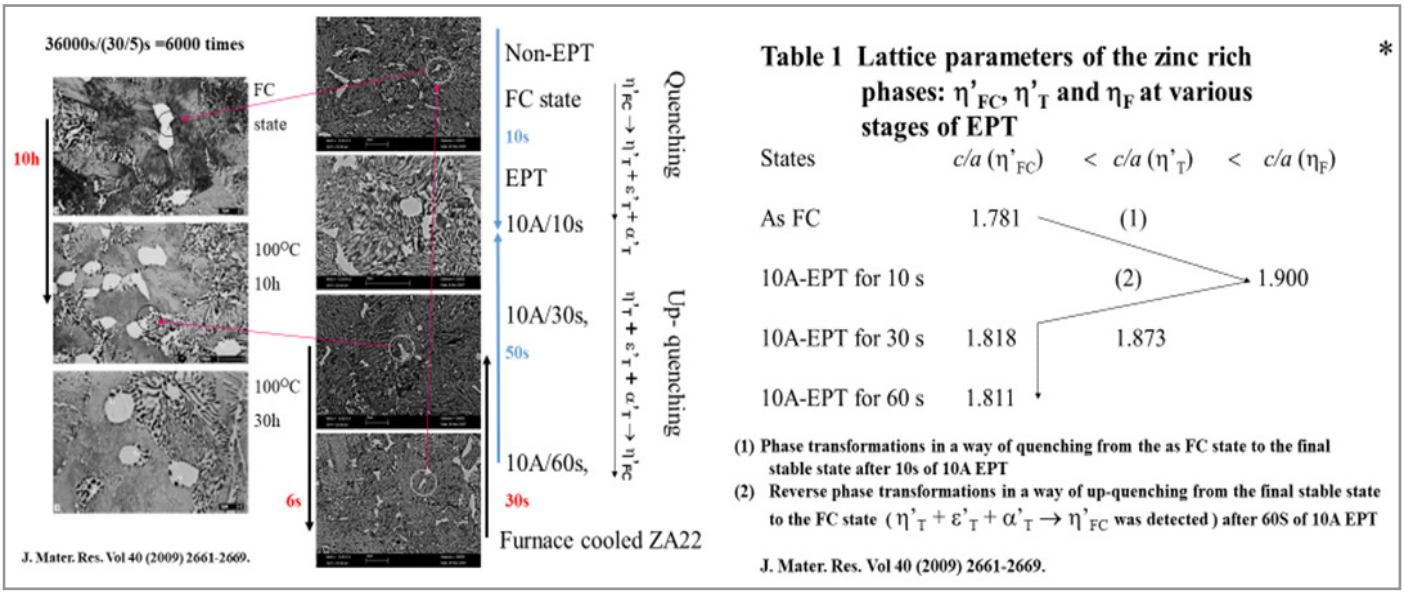

Table 1 Lattice parameters of the zinc rich phases: η'_{FC}, η'_T and η_F at various stages of EPT *

States	c/a (η'_{FC})	< c/a (η'_T)	< c/a (η_F)
As FC	1.781	(1)	
10A-EPT for 10 s		(2)	1.900
10A-EPT for 30 s	1.818	1.873	
10A-EPT for 60 s	1.811		

(1) Phase transformations in a way of quenching from the as FC state to the final stable state after 10s of 10A EPT

(2) Reverse phase transformations in a way of up-quenching from the final stable state to the FC state ($\eta'_T + \varepsilon'_T + \alpha'_T \rightarrow \eta'_{FC}$ was detected) after 60S of 10A EPT

J. Mater. Res. Vol 40 (2009) 2661-2669.

Figure 14: Electropulsing accelerated tremendously phase transformations of ZA22 alloy by factors of at least 6000 times.

Electropulsing induced circulation of phase transformation is shown in Figs.15,16. Correlation between the phase transformations in the aged and in the static EPT ZA27 alloys is studied and schematically shown in Fig.17 (ref. to Figs.15-16), where the reverse phase transformations are indicated by dashed lines.

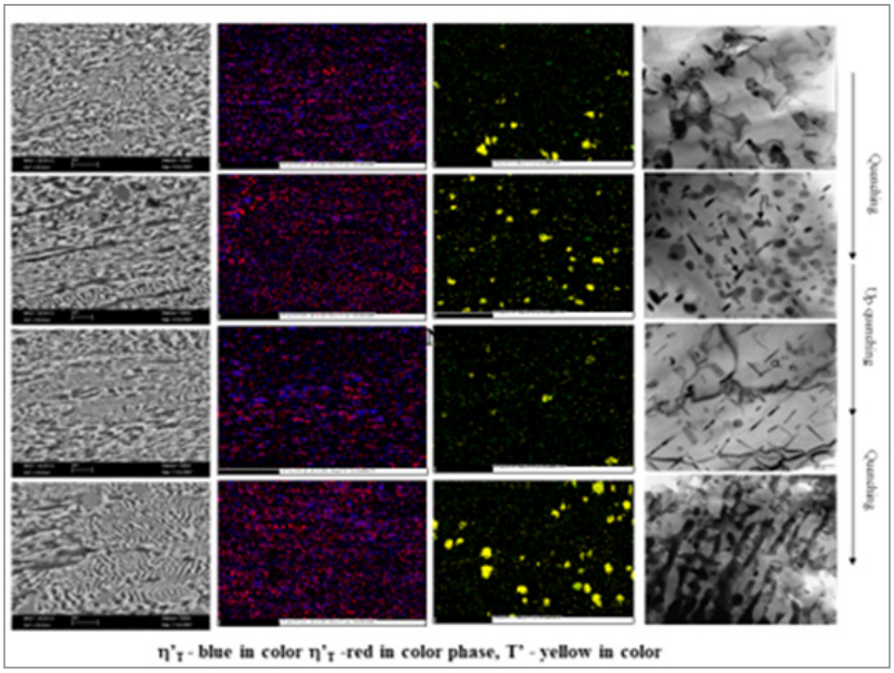

Figure 15: SEM, EBSD, TEM images to show circulation of transformations of ZA27 alloy.

It was found that the early stage of the electropulsing induced phase transformations (by a way of quenching) corresponded to those that occur in the early stage of ageing, while phase transformation that occurred in the prolonged stage of ageing could be induced in specimens at the later stage of EPT. Vise verse, the reverse phase transformations occurred in a way of up-quenching. Those phase transformations occurred in the prolonged stage of ageing takes place first, which were followed by the phase transformations occurred at the early stage of ageing, depending on the current density and the time of electropulsing.

It was the first time that the electropulsing induced 1.5-circular phase transformations (quenching up-quenching quenching) and preferred crystal orientation changes were quantitatively detected to complete within several seconds, in Zn-Al based alloys (Figs.14-17), Al-Mg alloys (Figs.18-21) and Fe-Si alloys (Fig. 22).

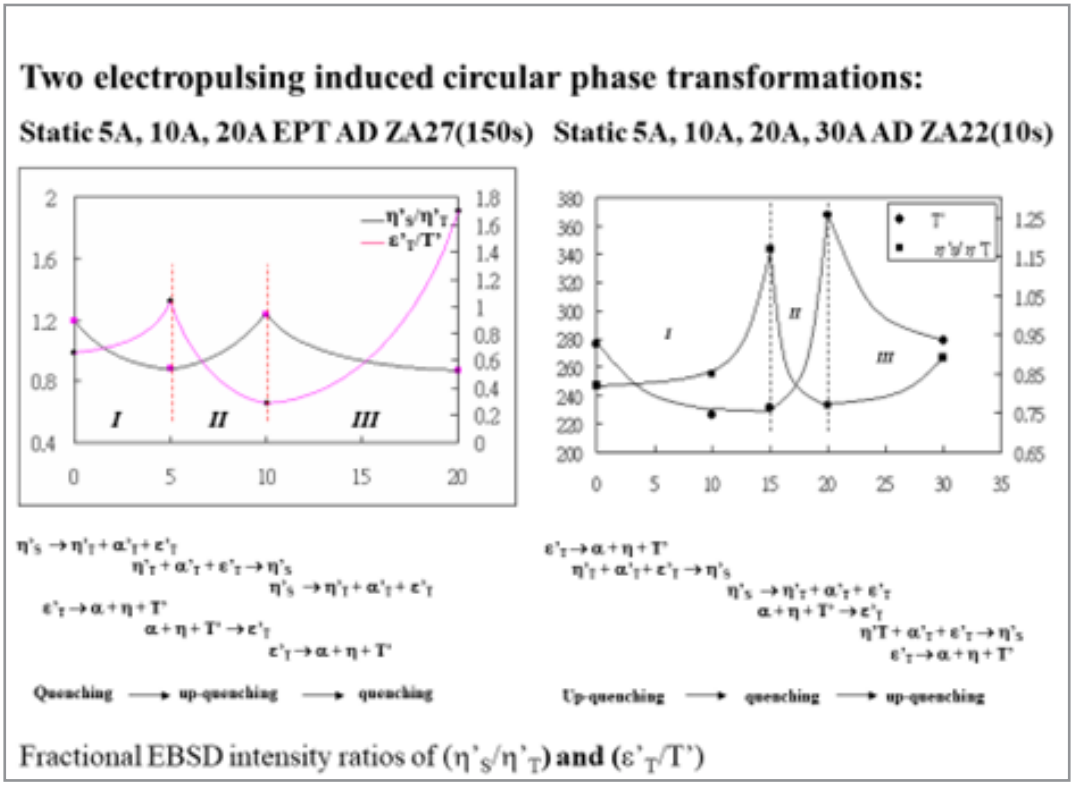

Figure 16: Circular transformations of ZA27 alloy were quantitatively detected.

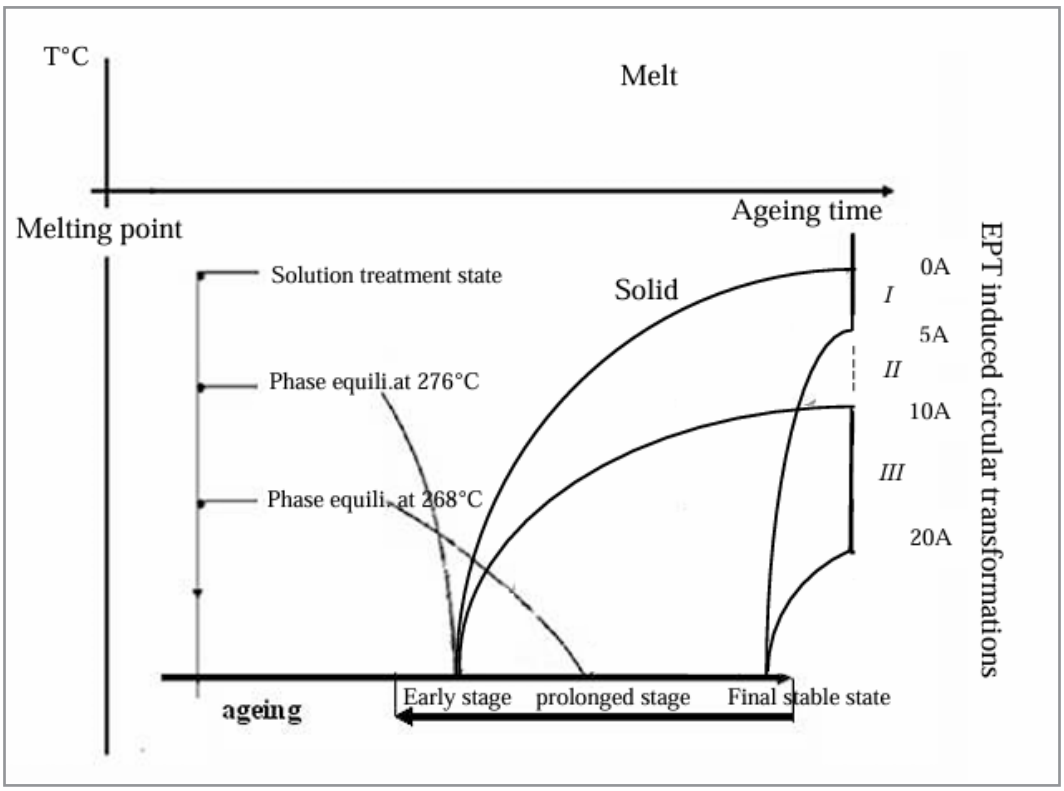

Figure 17: Correlation between the phase transformations in the aged and in the static EPT ZA27 alloys, where the reverse phase transformations are indicated by dashed lines, the EPT induced circular phase transformations as I, II and III.

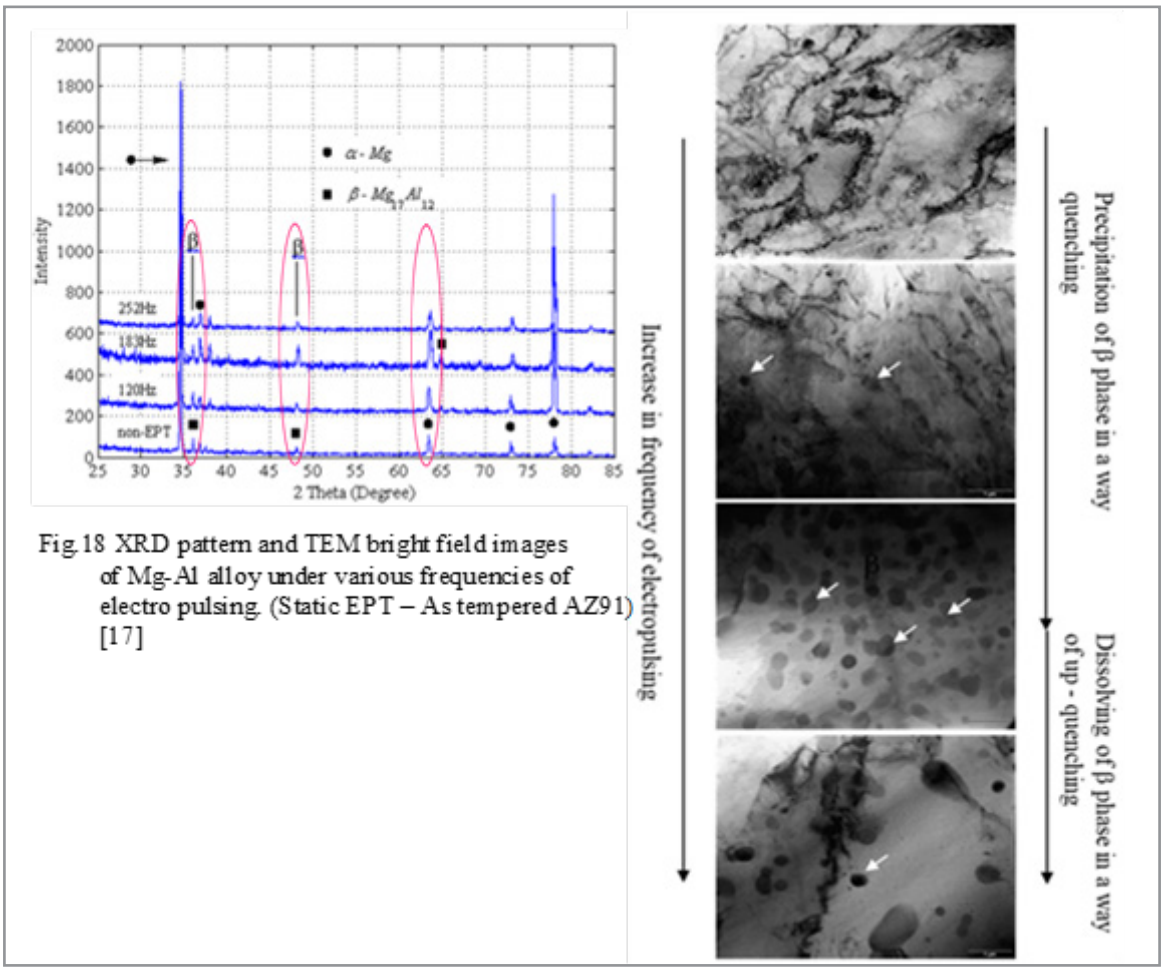

Fig.18 XRD pattern and TEM bright field images of Mg-Al alloy under various frequencies of electro pulsing. (Static EPT – As tempered AZ91) [17]

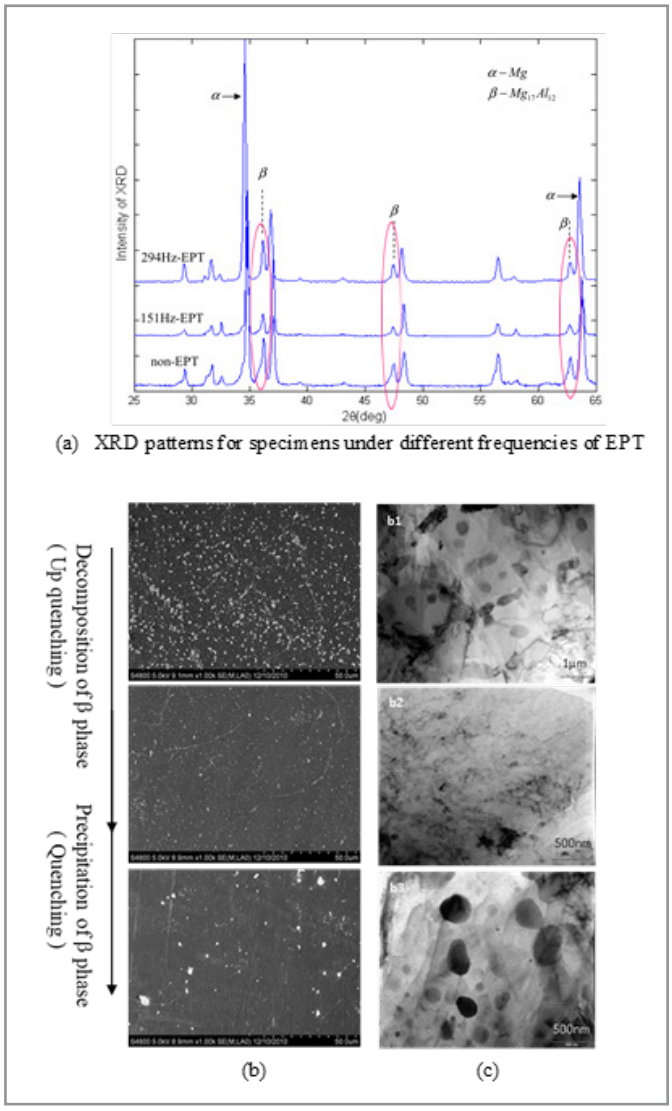

Figure 19: XRD (a), BSEM images (b) and TEM bright field images (c) of as deformed AZ91 specimens: (1) Non-EPT, (2) 151HzEPT, (3) 294Hz-EPT, showing β phase precipitates changes with various frequencies of electropulsing [18].

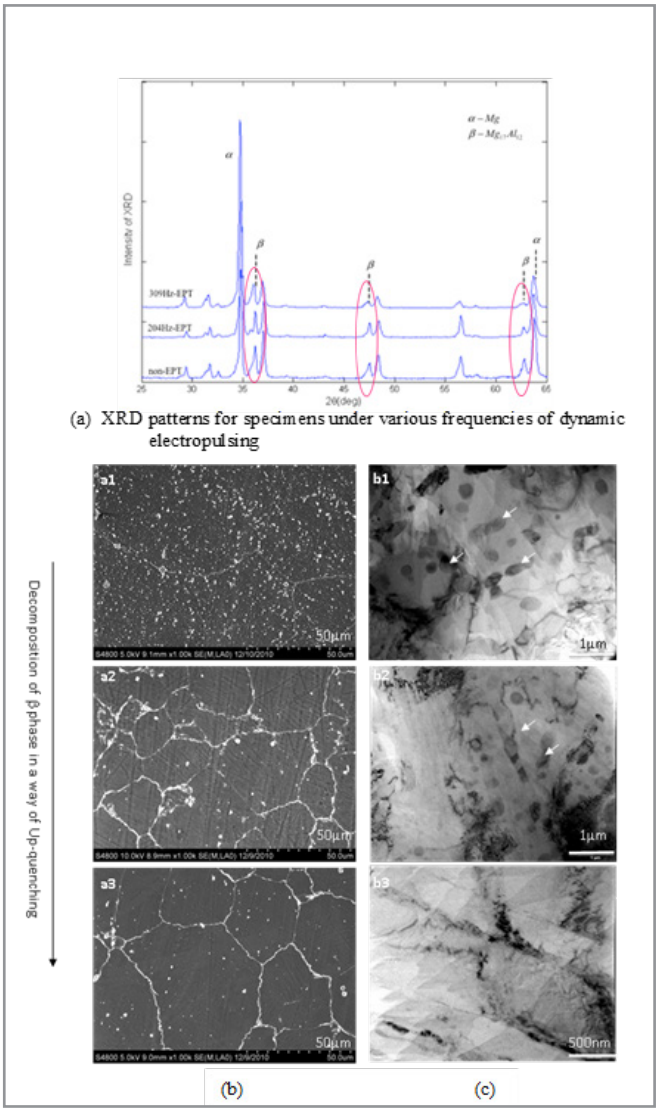

Figure 20: XRD (a), BSEM images (b) and TEM bright field images (c) of as deformed AZ91alloy specimens: (1) Non-EPT (2) 204HzEPT (3) 309Hz-EPT, showing β phase precipitates changes with various frequencies of electropulsing [19].

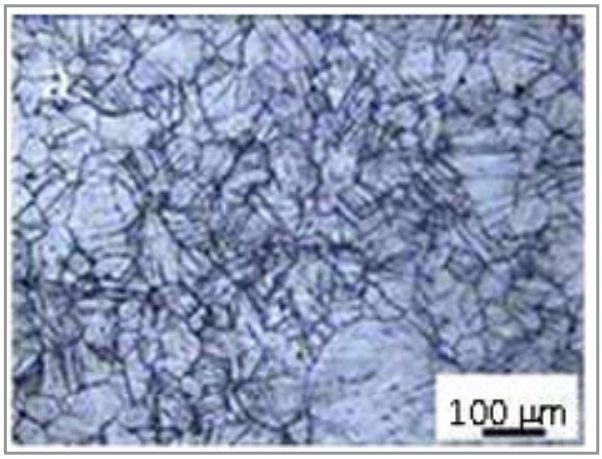

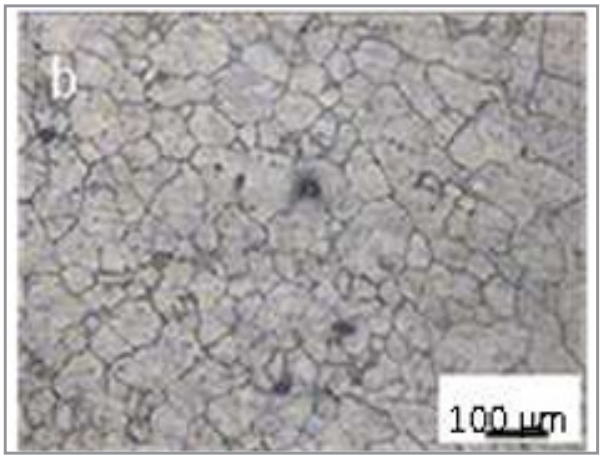

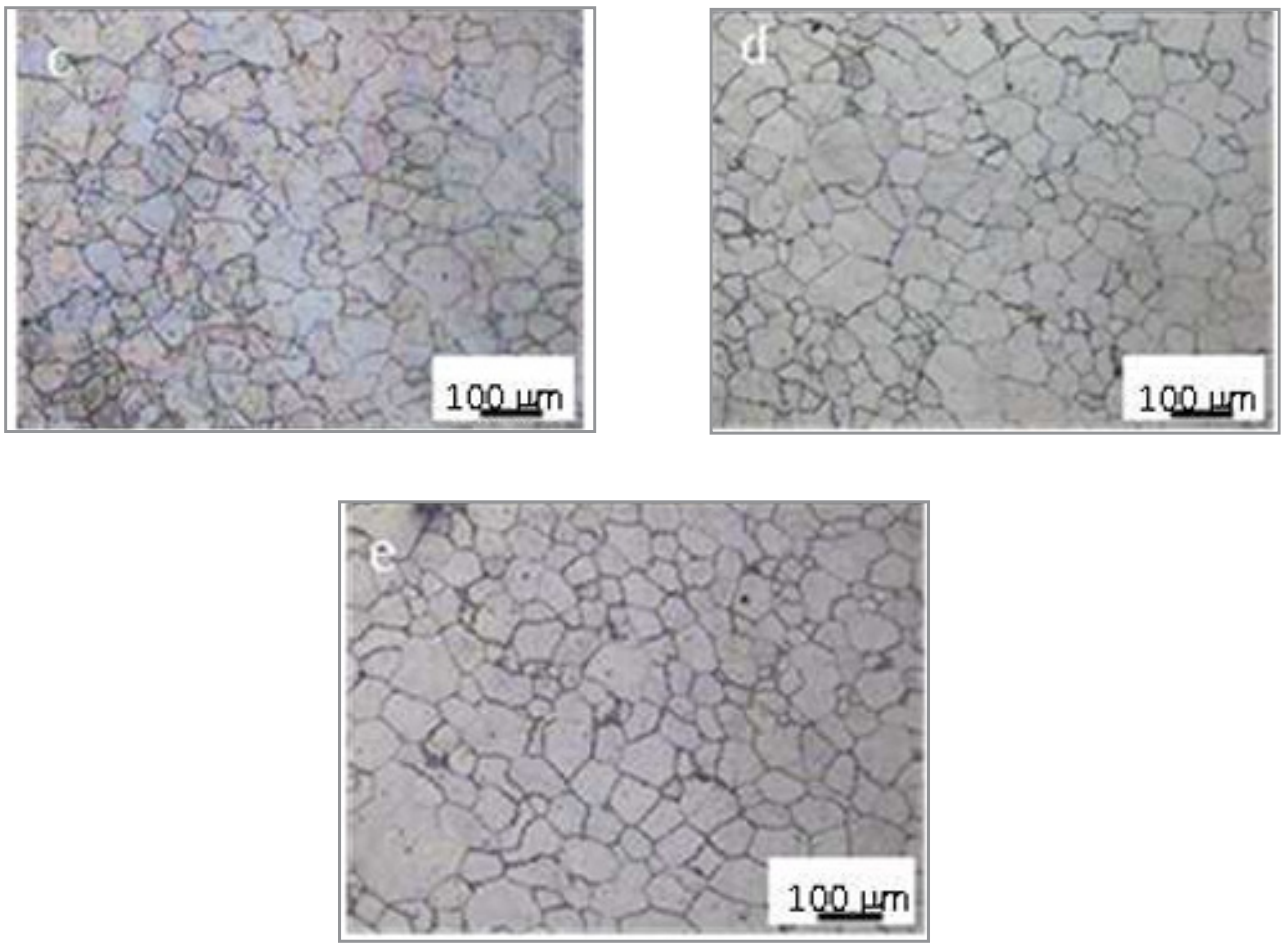

Figure 21: Optical micrographs of as deformed AZ91 specimens: (a) Non-EPT, (b) 126 Hz EPT and (c) 204 Hz-EPT, (d) 265Hz-EPT and (e) 309Hz-EPT.

Electropulsing tremendously accelerates texture evolution in recrystallization and decreases the temperature of the recrystallization of the cold rolled Fe-3Si alloy strip. [24-28] After several seconds of various steps of electropulsing, the alloy strip had been well recrystallized. The energy storage of the textures, i.e. the residual stress induced by the cold rolling was considerably reduced. Shown in Fig.22 are EBSD mapping (a), ODF figures (b), Euler mapping (c) and distribution of micro-orientation angles (d) of specimens after 3000Hz -EPTs: (1) 520°C. (2) 680°C, (3) 750°C, (4) 850°C, (5) 1000°C and (6) 1050°C.

Various textures with high energy storage, such as (001) <110>, (111) <112>, (111) <110> and G texture (110) <100>, formed after several seconds of EPT, depending on the intensity of the electropulsing.

Under electropulsing, the G-texture with high energy storage develops as increasing misorientation distribution of the low angle grain boundaries (2 10 degree). Shown in Fig.25 are EBSD mappings and ODF figures of annealed at (a)893K and (b)1123K for 20min and 12s-EPT (c) and (d) with various frequencies and temperatures for 98Hz/783K (c1, d1), 116Hz/ 8543K (c2, d2), 152Hz/1023K (c3, d3) and 173Hz/ 1123K (c4, d4), respectively.

Share bands with high distribution of the small misorientation, i.e. the low angle grain boundaries (2 degree), are not favorable in dislocation climbing and accumulation.

The driving force for recrystallization in the EPT alloy specimens consists of two parts, i.e. G = Gtherm + Gep, where ΔG thom is the Gibbs free energy resulting from Joule, Gep. is the electropulsing-induced Gibbs free energy, which is closely related to the crystal orientation. As for the evolution of the G-texture in the recrystallization, the athermal effect of electropulsing is 319 times stronger than the thermal effect of electropulsing

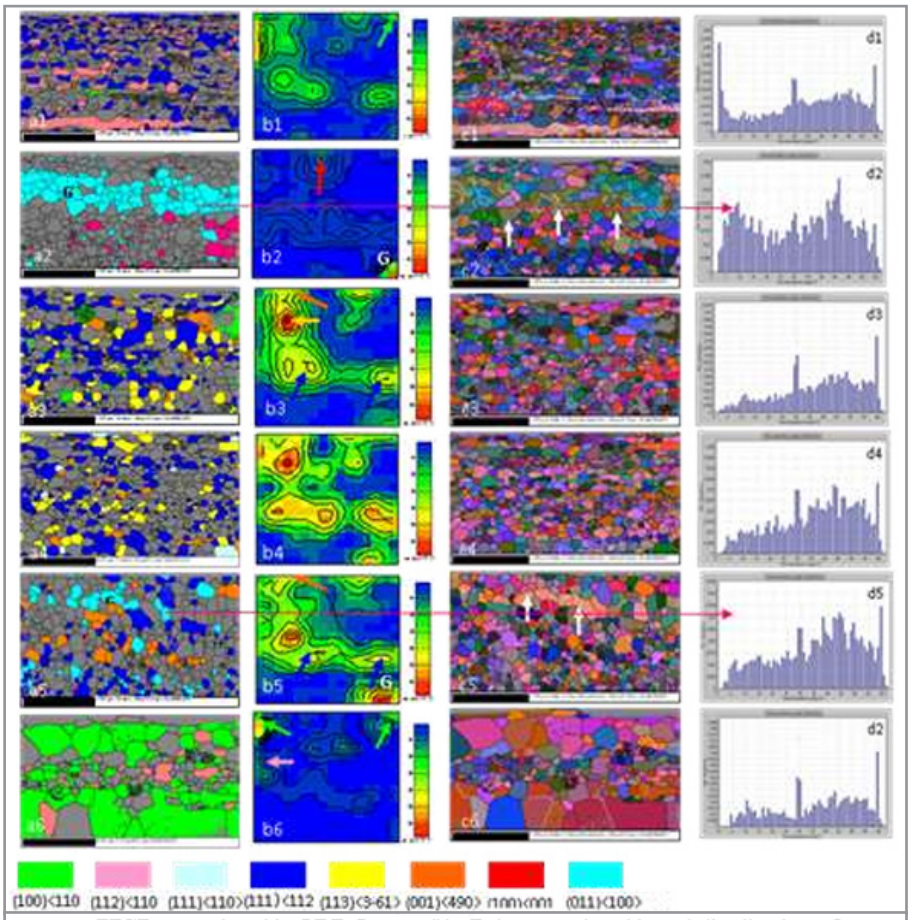

EBSD mapping (a), ODF figures (b), Euler mapping (c) and distribution of micro-orientation angles (d) of specimens after 3000Hz -EPTs: (1) 520°C. (2) 680°C, (3) 750°C, (4) 850°C, (5) 1000°C and (6) 1050°C.

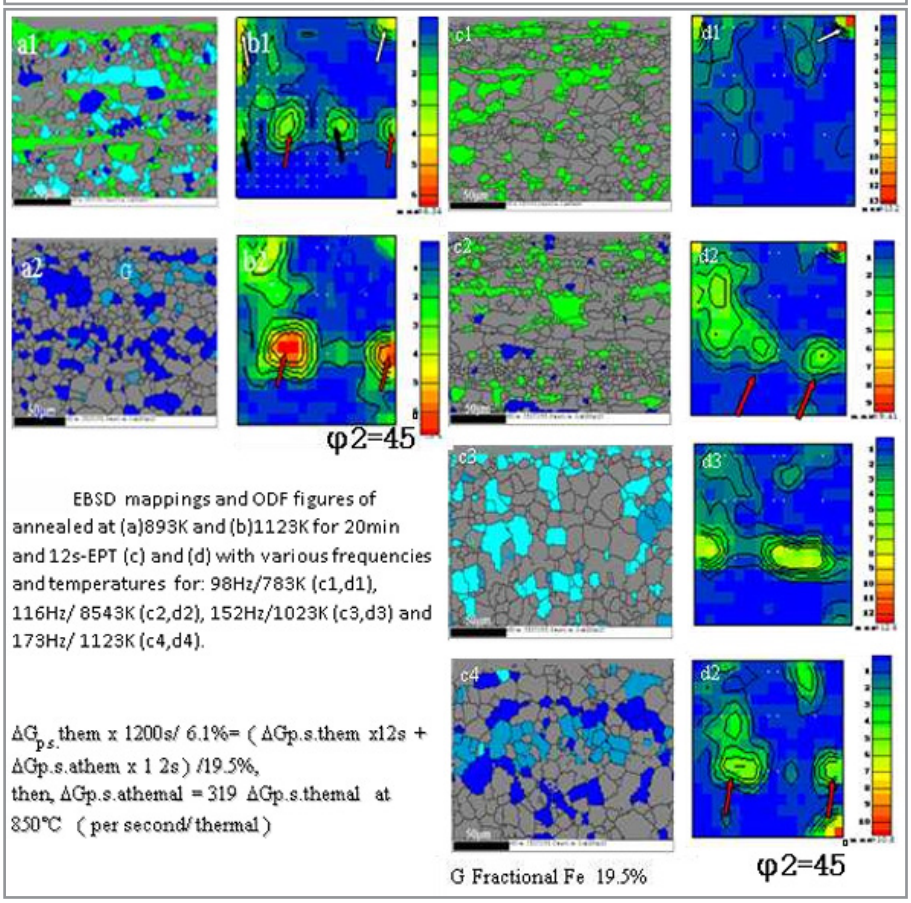

EBSD mappings and ODF figures of annealed at (a)893K and (b)1123K for 20min and 12s-EPT (c) and (d) with various frequencies and temperatures for: 98Hz/783K (c1,d1), 116Hz/ 8543K (c2,d2), 152Hz/1023K (c3,d3) and 173Hz/ 1123K (c4,d4).

$\Delta G_{p.s.}$ them x 1200s/ 6.1%= (ΔGp.s.them x12s + ΔGp.s.athem x 1 2s) /19.5%,
then, ΔGp.s.athemal = 319 ΔGp.s.themal at 850°C (per second/ thermal)

G Fractional Fe 19.5%

Figure 22: Electropulsing induced texture evolution of recrystallization in Fe 3%Si alloy. (ODF figures - Orientation Distribution Function figures) [37, 38].

It was the first time that the electropulsing induced two circles of phase transformation and preferred crystal orientation were detected in ways of (quenching up-quenching quenching up-quenching) in thin films of AZO and Bi-Te semiconductors, as shown in (Figs. 23, 24) [38].

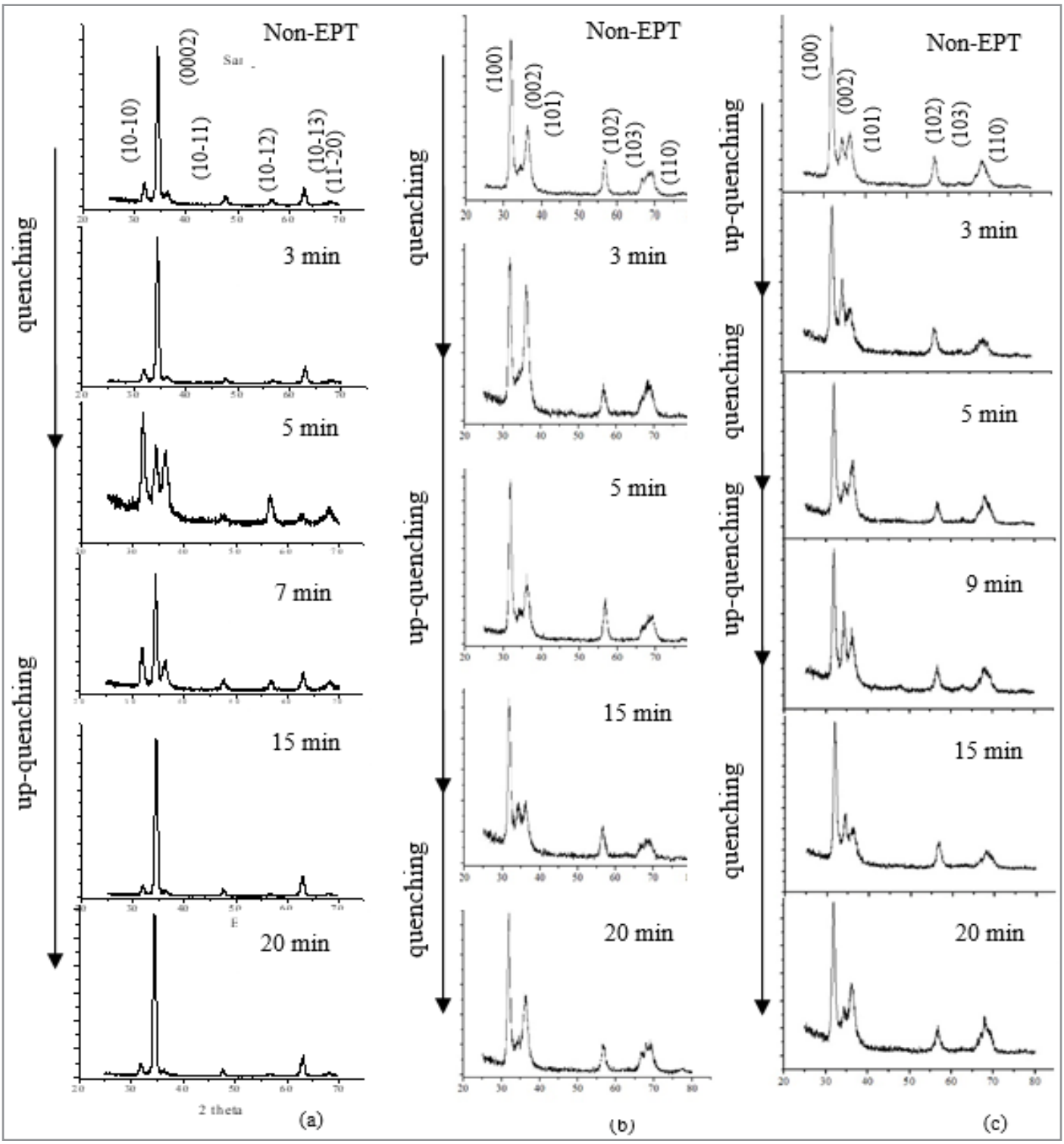

Figure 23: XRD showing multi-circulations of transformations and crystal orientation changes in EPT thin films of AZO-5 semiconductor

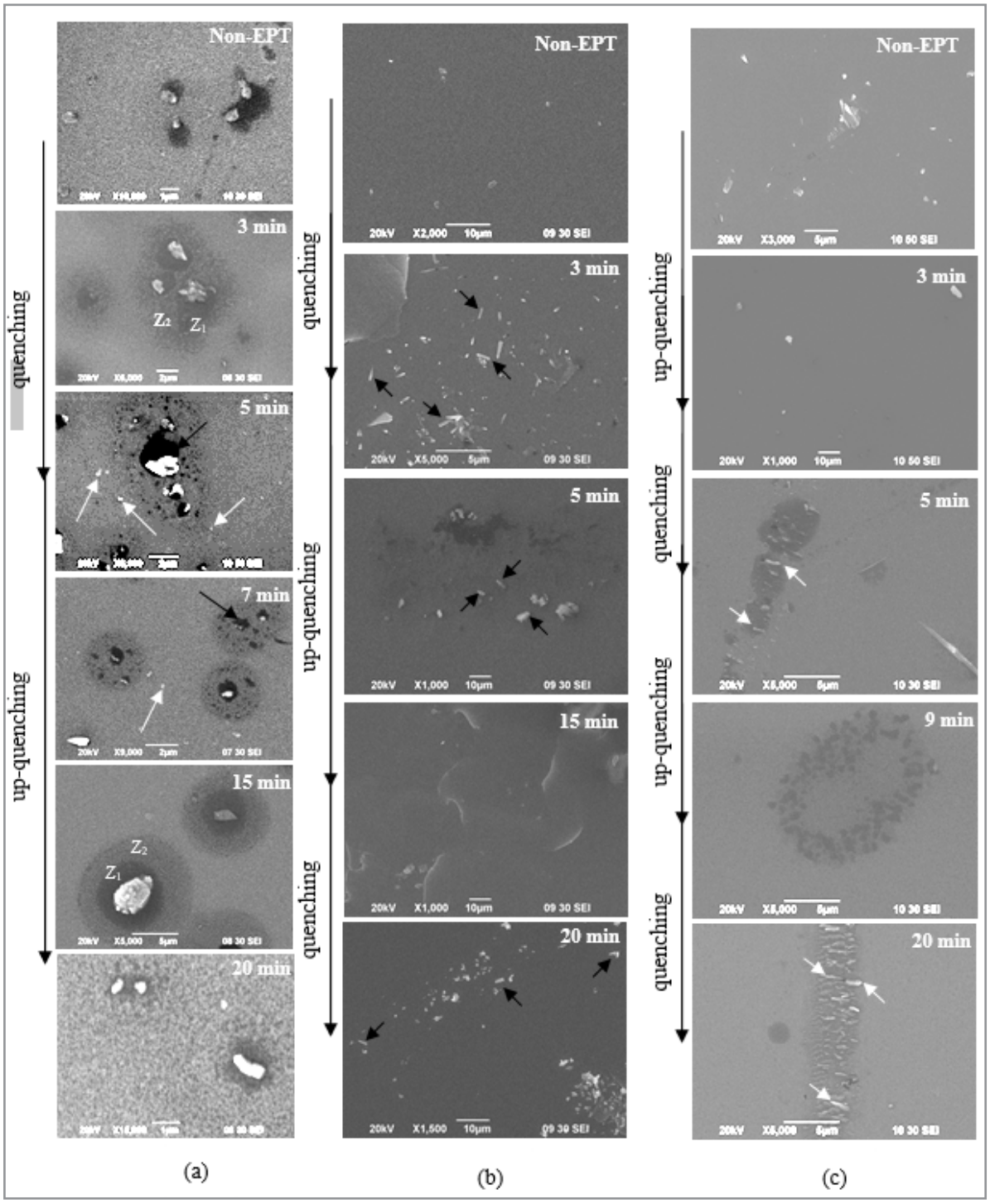

Figure 24: SEM showing multi-circulations of transformations and crystal orientation changes in EPT thin films of AZO-5 semiconductor

Adequate electropulsing increases THz reflection, electric conductivity and surface roughness of thin films of AZO2, (Figs.25-28) and conductivity of the thin films of AZO and Bi-Te for 18.5% and 28.5%, respectively [35-39].

The THz Time domain waveforms, i.e. THz reflection amplitude vs delay time, of AZO thin-films are shown in Fig.25. At early stage of electropulsing, the THz reflection rapidly increased with increasing time, and reached the maximum after electropulsing for 15 mins. The THz reflection increased by a factor of 22.8%, compared that of the as coated AZO-2 thin-films. Then THz reflection decreased during the prolonged electropulsing. The AZO-2 thin-films were of very effective THz responses within a wide range of THz band (0.1- 1.6 THz). After EPT for 15 mins, the terahertz waveforms of AZO films were very close to that of the standard Au mirror in the time domain, being over 96% of Au standard sample (100%), as indicated by a solid line in Fig.27. Outside this frequency range, the signal was too weak to obtain an acceptable signal-to-noise ratio in the terahertz system.

Within the THz frequency bands, the electromagnetic wave interacted with free carrier, and scattered within unit cells or defects such as dislocations, boundaries and voids etc., which would reflect the THz phonons. Thus, the THz reflection was

closely related to the microstructural defects, i.e. the carrier concentration in the AZO-2 thin- films.

The electropulsing induced THz reflection changes followed a similar circulation to that the electrical conductivity underwent. At the early stage of EPT, the significant increase in dislocation density and carrier concentration because of destroying the high- stressed preferred crystal orientation at the (0002) planes, and the THz reflection increased greatly. After EPT for 15 mins, the Al-precipitates considerably increased, accordingly the dislocation density and the carried concentration increased to the maximum. Accordingly, both the highest electrical conductivity and the strongest THz reflection were observed.

It can be seen that both the discontinuous secondary precipitation and the preferred crystal orientation changes accompanying decrease in stress favored enhancing both electrical conductivity and THz reflection in the AZO-2 thin-films, and vice versa. Destroying the high-stressed crystal orientation played an important role in enhancing the properties.

The quantitative detection of multi-circulation of both phase transformations and preferred crystal orientation changes makes it possible to monitor microstructural changes and to enhance physical and optical properties of the thin films.

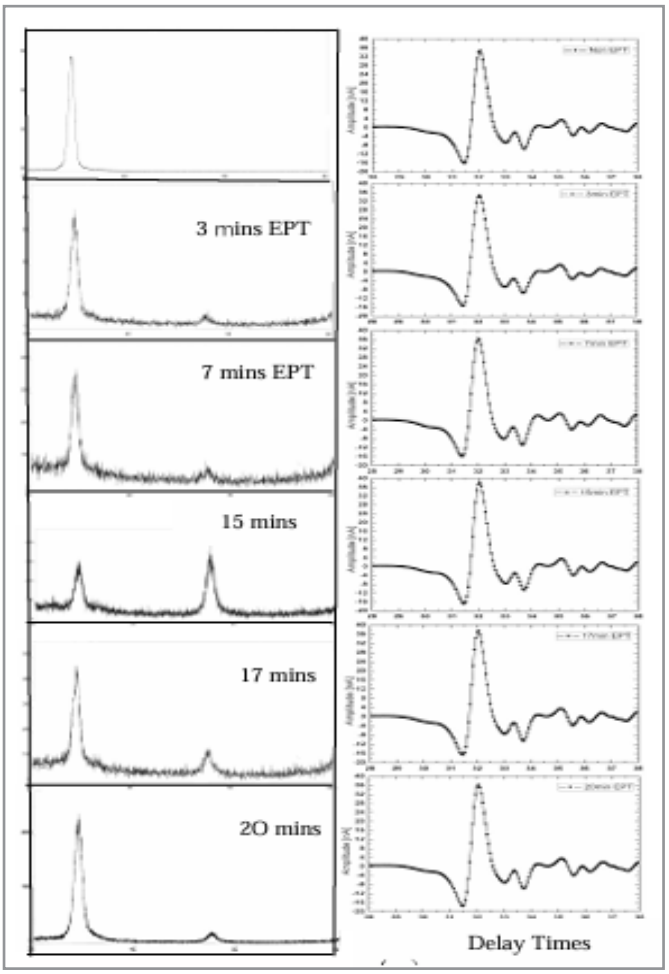

Figure 25: X-ray diffractograms (a) and THz reflection magnitude (b) of AZO2 thin films after various periods of EPT, 3, 7, 15, 17 and 20 mins, showing the second phase precipitates and the preferred crystal orientation at favored enhancing THz reflection.

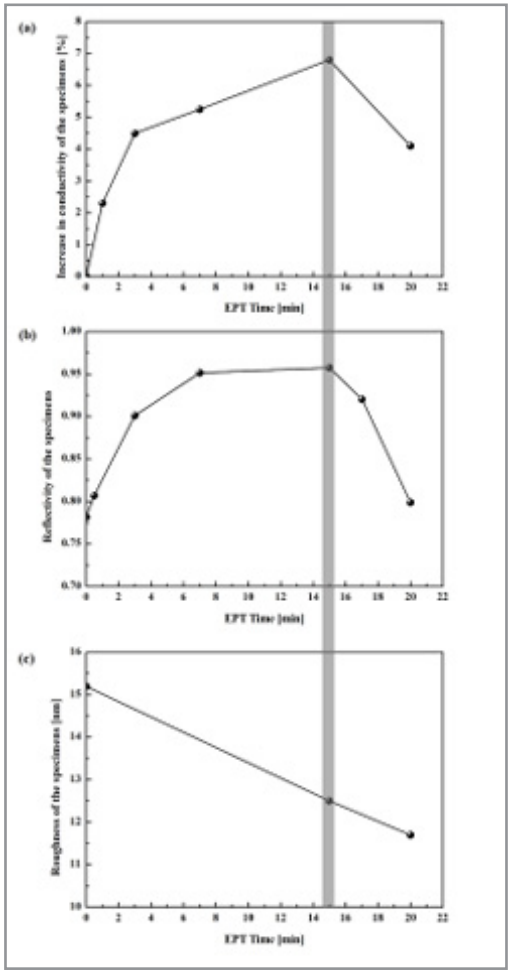

Figure 26: Relative increases of electrical conductivity (a), THZ reflectivity (b) and surface roughness (c) of AZO-2 thin films after various periods of electropulsing.

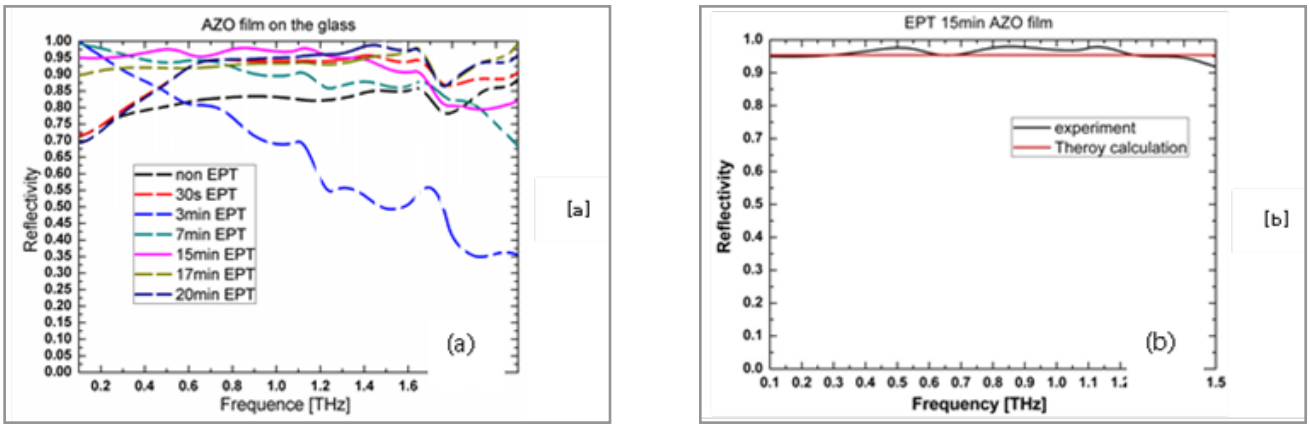

Figure 27: THz reflection amplitude vs delay time (a) and theoretical (grey) and experimental (dark) amplitude reflectivity (b) of the AZO-2 thin films.

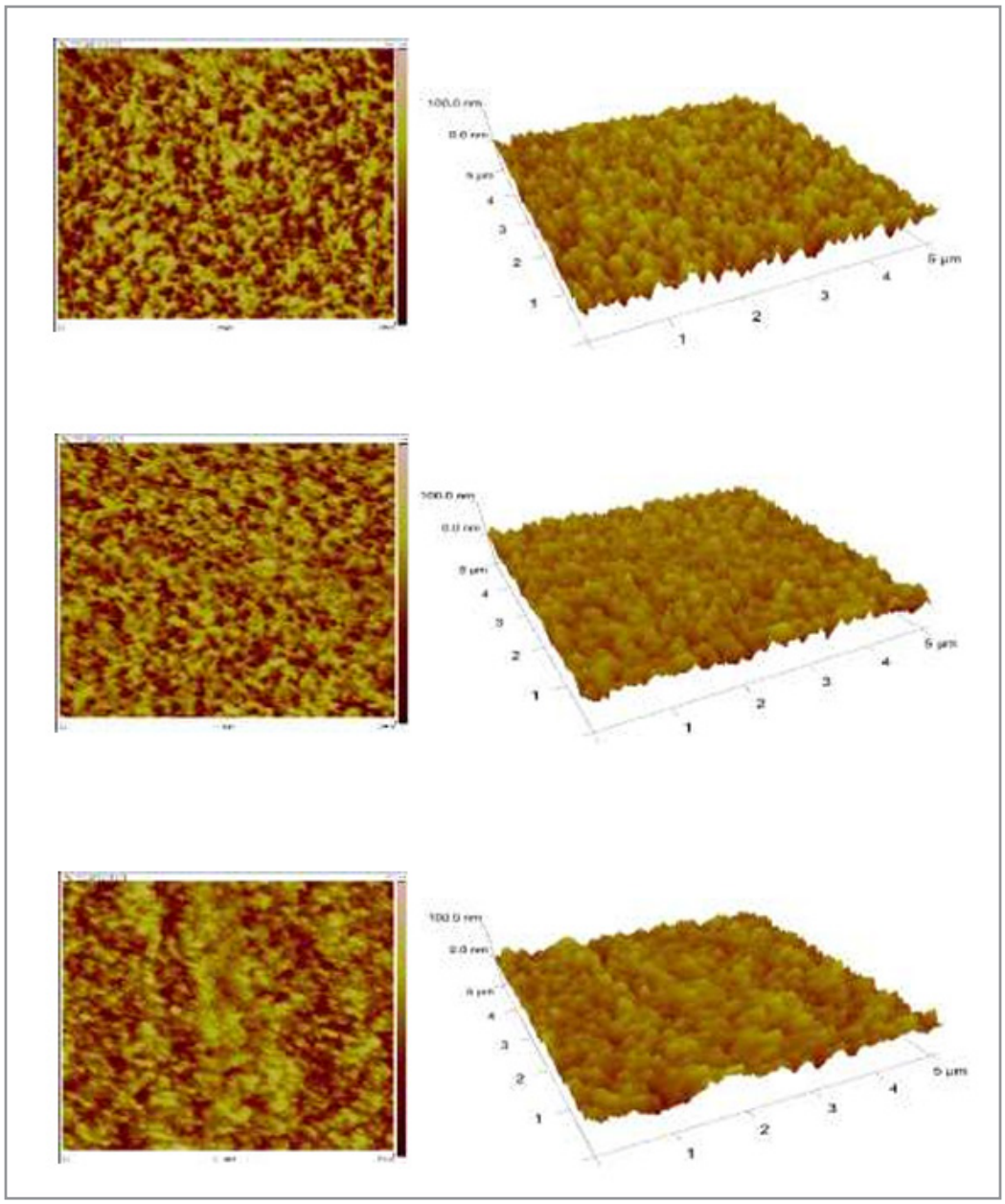

Figure 28: AFM images of the AZO-2 thin-films after EPT for 0 (a), 15 (b) and 20 (c) mins.

Conductivity responses of electropulsing in the thin films of Bi-Te and AZO semiconductors are shown in Fig.29. Comparison of age-hardening and the conductivity responses of electroplating is shown in Fig.30. It can be seen that the age-hardening (a) occurred due to formation of the transitional phases (b), and the conductivity responses of electropulsing (c) due to dislocation pinning of the continuous precipitates (d) [35-39].

It is concluded that phase decomposition (quenching) enhances conductivity, while reverse phase decomposition (up-quenching) decreases conductivity.

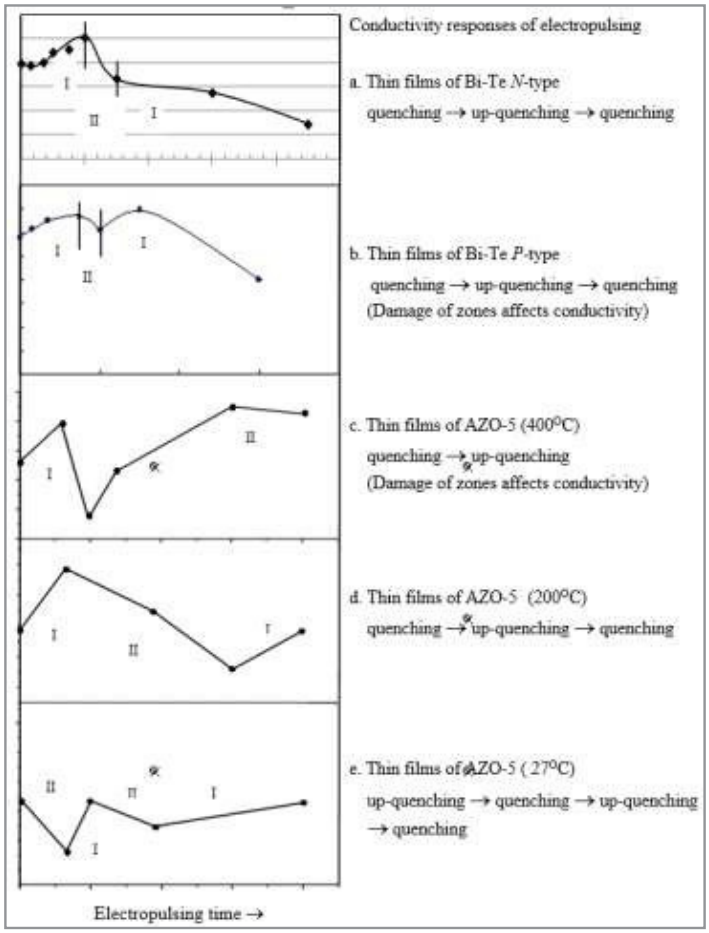

Figure 29: Conductivity responses of electropulsing

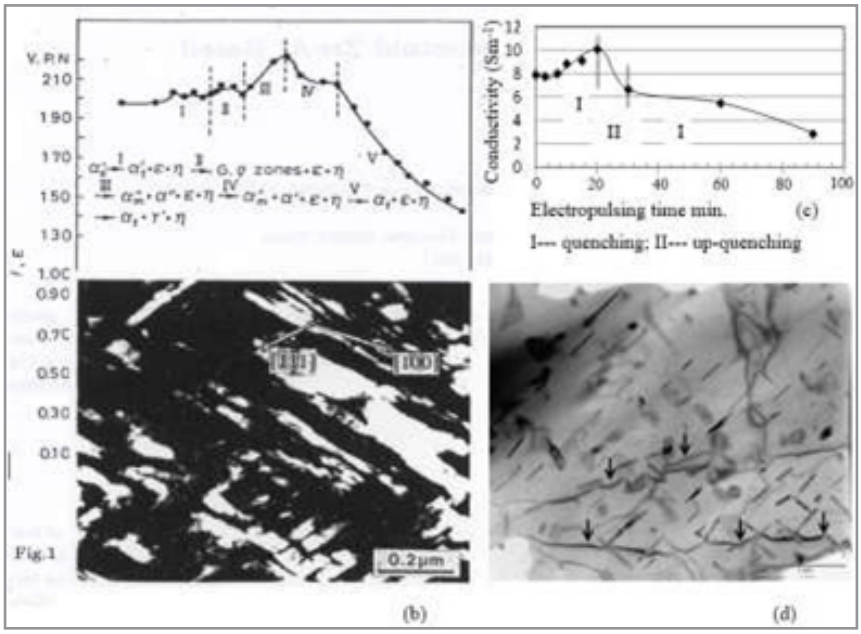

Figure 30: Comparison of age hardening and conductivity responses of electropulsing [38].

Physical and chemical properties of the semiconductors are stable, whilst the thin films of the semiconductors appear even more stable because of their strong preferred crystal orientation. Traditional thermal and stress processes are not strong enough in exploring structural evolution of the thin films of semiconductors. As an advanced processing, electropulsing appears a unique process in exploring microstructural changes, and enhancing physical properties of the thin films of semiconductors.

Based on the previous basic studies of electropulsing induced phase transformations in alloys and the thin films of the Bi-Te and AZO semiconductors, the co-relations between phase transformation and microstructural changes and those physical properties were well established. (Figs.29, 30)

The task of the present research and development proposal aims at practical application of the electropulsing to breakthrough the traditional temper-process to semiconductor related industries.

The well determined electropulsing processes will focus directly on the thin films which are currently applied in the semiconductor industries, solar energy, electronic communication and computation industries (such as TCO and TE, microchips etc.), in order to achieve the best properties, and upgrade the currently applied thin films, microchips and strips etc. to a new level in the huge market of the functional semiconductor industry.

Further research and development are proposed as follows,
a. Phase transformation and microstructural changes of thin films of semiconductors (in laboratory research),

1. Electropulsing processes for Transparent conductive oxide (TCO), such as AZO, ITO etc.,
2. Electropulsing processes for GeR (R= Sn,Bi,Si),
3. Electropulsing for Quantum thin films.

b. Research and development of application processes in industry of semiconductors.

Pilot plant research and work out the appropriate EPT processes in the practical product lines. For those small dimensional thin film products, the appropriate EPT process shall be directly applied in the production lines in industry).

A research road map went through various aspects of physical metallurgy, including thermal metallurgy, mechanical metallurgy, electro-metallurgy and electro-mechanical metallurgy, was scientifically logical and effective in studying and exploring applications of the thin films of semiconductors, as shown in Fig.31.

The systematical investigations of physical metallurgy were carried out through the research road map as follows,

1. equilibrium phase diagrams
2. non-equilibrium phase transformations
3. external stress induced phase transformations
4. electropulsing induced phase transformations in alloys
5. electropulsing induced phase transformations in thin films of alloys
6. electropulsing induced phase transformations in thin films of semiconductors.

It is of great theoretical importance and practical significance to study the fundamental mechanism by which such significant changes of phase transformations and their effects on the plastic behaviors and electric conductivity of the alloys and the thin films of semiconductors were obtained.

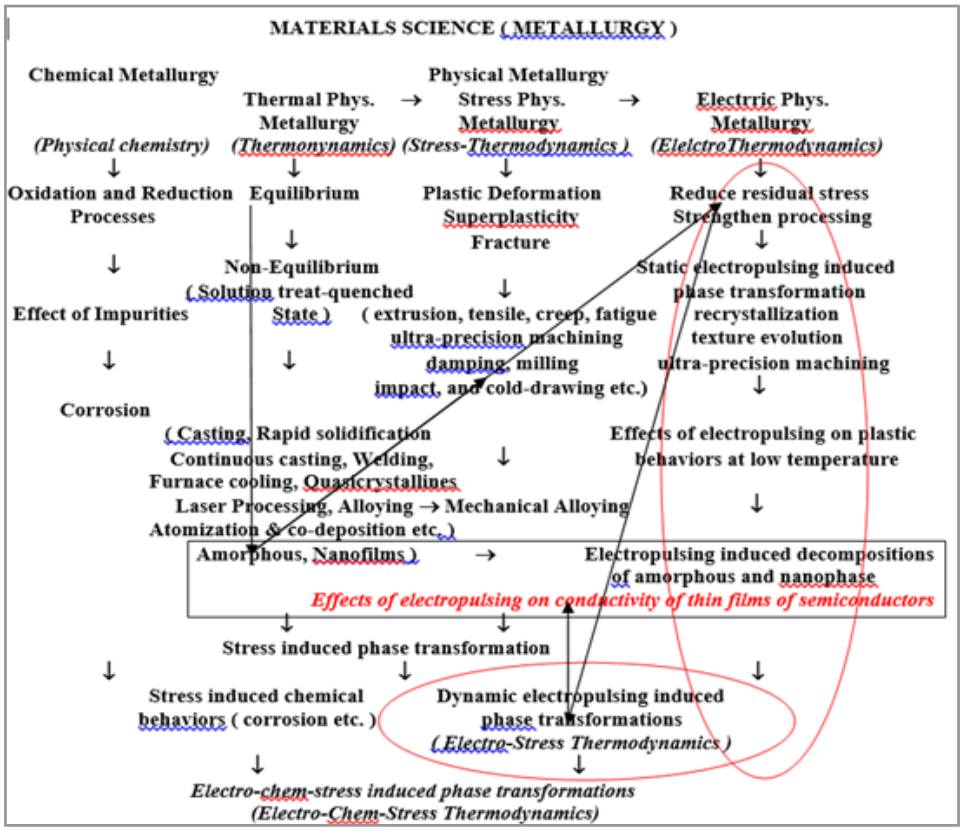

Figure 31: Schematic research road map approaching thin films of semiconductors (TCO and TE)

Conclusions

In summary, General rule of phase transformations (IV) --- On electropulsing induced phase transformations in thin films of Bi-Te and AZO semiconductors were worked as follows, [38, 39]

1. Electropulsing accelerated phase transformations tremendously of the thin films of ZA alloy and Bi-Te semiconductors.
2. Electropulsing induced circulation of phase transformations occurred by ways of quenching and up-quenching (quenching → up-quenching; quenching → up quenching → quenching; …up-quenching → quenching → up-quenching → quenching etc.).
3. The substrate temperature affected electropulsing induced phase transformations considerably.
4. The electropulsing induced preferred crystal orientation changes were closely related to the phase transformations in the EPT thin films of semiconductor.
5. Electrical conductivity responses of electropulsing were closely related to the electropulsing induced phase transformation and the preferred crystal orientation in the sputtering deposited thin films of the alloys and TCO and TE semiconductors.
6. Electropulsing improved THz reflections, PL reflections, and surface roughness of the thin films of Bi-Te and TE semiconductors

Acknowledgement

The author would like to express his gratitude to The Hong Kong Polytechnic University for financial support and also to M.N. Yeung of Materials Research Center of The Hong Kong Polytechnic University and Mr. F.Y.F Chan of the Electron Microscopy Unit of the Hong Kong University for their help in conducting the experimental work. The author also wishes to express his gratefulness to all co-authors who have appeared in these research articles, without whom this book would not have been completed.

References

1. Zhu, Y. H. (1989). Phase equilibria in Zn-Al-Cu-Si system at 285°C. Chinese Journal of Metallurgical Science and Technology, 5, 113-118.
2. Zhu, Y. H., Murphy, S., & Yeung, C. F. (1999). Early stage of phase transformation in quenched zinc-aluminum-based alloys. Journal of Materials Processing Technology, 94, 78-84.
3. Zhu, Y. H., & Torres, J. (1997). Tensile deformation in extruded eutectoid Zn-Al based alloy. Zeitschrift für Metallkunde, 88, 329-332.
4. Zhu, Y. H., & Lee, W. B. (2000). Tensile deformation and phase transformation of furnace-cooled Zn-Al based alloy. Materials Science and Engineering A, 293, 95-101.
5. Zhu, Y. H. (2004). General rule of phase decomposition in Zn-Al based alloys (II) – On effect of external stress on phase transformation. Materials Transactions JIM, 45(11), 3083-3097.
6. To, S., Lee, W. B., & Zhu, Y. H. (2002). Ultra-precision machining induced surface structural changes of Zn-Al alloy. Materials Science and Engineering A, 325, 497-502.
7. Zhu, Y. H., To, S., Lee, W. B., Zhang, S. J., & Cheung, C. F. (2010). Ultra-precision raster milling induced phase decomposition and plastic deformation at the surface of a Zn-Al alloy. Scripta Materialia, 62, 101-104.
8. Zhu, Y. H., To, S., Lee, W. B., Liu, X. M., Jiang, Y. B., & Tang, G. Y. (2009). Effect of dynamic electropulsing on microstructure and elongation of a Zn-Al based alloy. Materials Science and Engineering A, 501, 125-132.
9. Zhu, Y. H., To, S., & Liu, X. M. (2012). Influence of spinodal decomposition on plastic behavior of dynamic electropulsing treated ZA22 alloy. Materials Transactions JIM, 53(8), 1363-1370.
10. Zhu, Y. H., To, S., & Liu, X. M. (2011). Effects of static electropulsing on behaviors of a Zn-Al based alloy (ZA22). Metallurgical and Materials Transactions A, 42A(7), 1933-1940.
11. To, S., Zhu, Y. H., Lee, W. B., Liu, X. M., & Jiang, Y. B. (2009). Effects of current density on elongation of an electropulsing treated Zn-Al based alloy. Materials Transactions JIM, 50(12), 2772-2777.
12. Zhu, Y. H., To, S., Lee, W. B., Liu, X. M., Jiang, Y. B., & Tang, G. Y. (2009). Electropulsing induced phase transformation in a Zn-Al based alloy. Journal of Materials Research, 24, 2661-2669.
13. Zhu, Y. H., To, S., & Liu, X. M. (2011). Use of EBSD to study electropulsing induced reverse phase transformations in a Zn-Al based alloy. Journal of Microscopy, 242, 62-69.
14. Zhu, Y. H., To, S., Liu, X. M., Hu, G. L., & Xu, Q. (2011). Static electropulsing induced phase transformations in cold deformed ZA27 alloy. Journal of Materials Research, 26(4), 1696-1701.
15. Zhu, Y. H., Jiang, Y. B., & Liu, X. M. (2018). Electropulsing induced circular phase transformation in a cold deformed Zn-Al based alloy (ZA27). Journal of Alloys and Compounds, 373, 630-636.
16. Zhu, Y. H., Jiang, Y. B., & Liu, X. M. (2018). Electropulsing induced circular phase transformation in a cold deformed Zn-Al based alloy (ZA27). Journal of Alloys and Compounds, 737, 630-636.
17. Jiang, Y. B., Tang, G. Y., Shek, C. H., Zhu, Y. H., Guan, L., Wang, S. N., & Xu, Z. H. (2009). Improved ductility of aged Mg-9Al-1Zn alloy strip by electropulsing treatment. Journal of Materials Research, 24(5), 1810-1814.
18. Jiang, Y. B., Tang, G. Y., Shek, C. H., & Zhu, Y. H. (2009). Effects of electropulsing on microstructure and tensile fracture behaviors of Mg-9Al-1Zn alloy strip. Applied Physics A, 97(3), 607-615.
19. Jiang, Y. B., Tang, G. Y., Shek, C. H., Zhu, Y. H., Guan, L., Wang, S. N., & Xu, Z. H. (2008). Effect of electropulsing treatment on solid solution behavior of aged AZ61 alloy strip. Journal of Materials Research, 23, 2685-2691.
20. Jiang, Y. B., Tang, G. Y., Shek, C. H., & Zhu, Y. H. (2009). On the thermodynamics and kinetics of electropulsing induced dissolution of β-Mg17Al12 phase in an aged Mg-9Al-1Zn alloy. Acta Materialia, 57, 4797-4808.
21. Zhang, D., To, S., Zhu, Y. H., Wang, H., & Tang, G. Y. (2012). Electropulsing induced β phase transformations and their effect on ultra-precision machining of a tempered alloy (AZ91) sheet. International Journal of Materials Research (Zeitschrift für Metallkunde), 21, 1205-1209.

22. Zhang, D., To, S., Zhu, Y. H., Wang, H., & Tang, G. Y. (2012). Static electropulsing induced microstructural changes and their effects on ultra-precision machining of a cold-rolled alloy AZ91. Metallurgical and Materials Transactions A, 43(4), 1341-1346.
23. Zhang, D., To, S., Zhu, Y. H., Wang, H., & Tang, G. Y. (2012). Dynamic electropulsing induced phase transformations and their effects on ultra-precision machining of a cold-rolled alloy AZ91. Journal of Surface Engineered Materials and Advanced Technology, 2(1), 16-21.
24. Hu, G. L., Tang, G. Y., Zhu, Y. H., & Shek, C. H. (2010). Effect of electropulsing on recrystallization Si alloy strip. Materials Transactions JIM, 51(8), 1390-1394.
25. Hu, G. L., Zhu, Y. H., Shek, C. H., & Tang, G. Y. (2011). Electropulsing induced G-texture evolution in a deformed Fe-3%Si alloy strip. Journal of Materials Research, 26(7), 917-922.
26. Hu, G. L., Tang, G. Y., Zhu, Y. H., & Shek, C. H. (2011). Electropulsing induced texture evolution in the recrystallization of Fe-3%Si alloy strip. Metallurgical and Materials Transactions A, 42(11), 3484-3490.
27. Hu, G. L., Wang, Z. T., Zhu, Y. H., Liu, J. A., & Tang, G. Y. (2011). Dynamic electropulsing induced evolution of basal texture and its effect on properties of magnesium alloy AZ61. Materials Transactions JIM, 52(8), 1565-1568.
28. Hu, G. L., Zhu, Y. H., Tang, G. Y., Shek, C. H., & Liu, J. N. (2012). Effect of electropulsing on recrystallization and mechanical properties of non-oriented silicon steel strip. Journal of Materials Science & Technology, 27(11), 1034-1038.
29. Yan, J., Liu, G., Zhao, X., & Shen, Y. (2021). Rapid homogeneous precipitation of nano-sized Si in Al–1% Si alloy by electric pulses. Materials Science and Technology, 37, 144-150.
30. Yan, J., Li, W., Liu, H., & Shen, Y. (2019). Reversion of sub-boundaries into dense dislocations in aluminum by electric pulsing treatment. Scripta Materialia, 167, 86-90.
31. Li, W., Shen, Y., Liu, H., Wang, Y., Zhu, W., & Xie, C. (2016). Non-octahedral-like dislocation glides in aluminum induced by athermal effect of electric pulse. Journal of Materials Research, 31, 1193-1200.
32. Li, W., Shen, Y. (2015). Effects of electric pulse on the annealing-induced hardening behavior of submicron grained Cu. Materials Science and Technology (UK), 31, 1577-1582.
33. Zeng, W., Shen, Y., Zhang, N., Huang, X., Wang, J., Tang, G., & Shan, A. (2012). Rapid hardening induced by electric pulse annealing in nanostructured pure aluminum. Scripta Materialia, 66, 147-150.
34. Zhu, Y. H., Jiang, S. Q., Zhao, D. D., Cheng, G. J., Zhang, H. W., & Lai, W. E. (2013). Electropulsing induced microstructural change and its effects on conductivity of nanofilms of Zn-Al alloys. Applied Physics A, 111(4), 1241-1245.
35. Zhu, Y. H., Jiang, J., Xiao, Y. K., Luk, C. M., & Lai, W. E. (2013). Electropulsing induced microstructure evolution and its effect on electrical conductivity of (Bi0.25Sb0.75)2Te3 thin films. Scripta Materialia, 69, 219-222.
36. Lai, W. E., Zhu, Y. H., Zhang, H. W., & Wen, Q. Y. (2013). A novel reflector of AZO thin films applicable for terahertz devices. Optical Materials, 35, 1218-1221.
37. Zhu, Y. H., & Lai, W. E. (2016). Effects of electropulsing induced microstructural changes on THz-reflection and electrical conductivity of Al-doped ZnO thin-films. Journal of Surface Engineered Materials and Advanced Technology, 6, 106-117.
38. Zhu, Y. H. (2018). Research road map approaching thin films of TCO and TE semiconductors, Part 2. On electropulsing induced phase transformations in thin films of Bi-Te and AZO semiconductors. Lambert Academic Publishing, pp. 48-54.
39. Zhu, Y. H. (2018). Research road map approaching thin films of TCO and TE semiconductors, Part 2. On electropulsing induced phase transformations in thin films of Bi-Te and AZO semiconductors. Lambert Academic Publishing, pp. 21-32.